SOME ASPECTS OF INCLUSIVE

NUCLEON PRODUCTION PROCESSES

by

JALALEDDIN PASHAIE-RAD

A thesis presented for the
degree of Doctor of Philosophy of the
University of London

T
BQE
Pas
139961
Jan 78

Department of Mathematics,
Royal Holloway College,
Englefield Green,
Surrey, TW20 0EX

March 1977

ProQuest Number: 10097438

All rights reserved

INFORMATION TO ALL USERS
The quality of this reproduction is dependent upon the quality of the copy submitted.

In the unlikely event that the author did not send a complete manuscript
and there are missing pages, these will be noted. Also, if material had to be removed,
a note will indicate the deletion.

ProQuest 10097438

Published by ProQuest LLC(2016). Copyright of the Dissertation is held by the Author.

All rights reserved.
This work is protected against unauthorized copying under Title 17, United States Code.
Microform Edition © ProQuest LLC.

ProQuest LLC
789 East Eisenhower Parkway
P.O. Box 1346
Ann Arbor, MI 48106-1346

Page

APPENDICES

CHAPTER ONE

GENERAL BACKGROUND

1.1 INTRODUCTION

The study of particle production processes[1,2] has attracted the interest of both theoretical and experimental elementary particle physicists in recent years. From the experimental point of view this seems natural, since production processes build up about 80% of the total cross section[3]. However, for the complex structure of the multiparticle production processes, parallel advances in both experimental and theoretical aspects were needed to sustain this interest. As a good example of this parallel advancement in the past few years, we may recall the proposal of a fourth quark and the discovery of the new particles, ψ/J, as the bound state.

The complexity of multiparticle scattering is due to the fact that the number of independent invariants is $3n - 10$[4], where n is the number of particles involved in the scattering, so there are only two invariants for four particle processes, while there are five and eight invariants for five and six particle processes, respectively. Experimentally it is very difficult to control many independent variables simultaneously and, therefore, processes of this type are not of interest. Nevertheless, it is possible to study multiparticle scattering in certain regions of phase space by choosing the appropriate kinematics and dynamics. Regarding dynamics there are two different approaches; one approach is to observe all the particles involved in the scattering. This is called the exclusive approach. Experiments of this type are difficult to carry out if there are more than five particles

involved in the scattering. The second approach, which is called the inclusive approach, is the one in which only a selective set of particles is observed, and was found extremely helpful in the investigation of production processes[5]. Experimentally, the inclusive approach means there are fewer variables to be controlled and therefore a simpler set up for carrying out the experiment and eventually the collection of data becomes a practical reality[6].

The interest in investigating the inclusive processes was further stimulated by the scaling hypothesis of Feynman[7], which can be traced back to the ABFST model[8] which leads to a similar result and was supported by experiments in the ISR range of energies[9].

Also, the limiting fragmentation hypothesis of Benecke et al.[10] suggests that the high energy processes look simple when viewed in the target or the projectile frame of reference. Finally, Regge analysis was introduced into inclusive processes through Mueller's generalized optical theorem[11] and inclusive Regge phenomenology has developed[2,12,13].

The construction of an explicit multi-Regge model as a basis of one-particle-inclusive phenomenology is presented in this thesis. The model with pure Regge poles is applied to the study of the charge-exchange nucleon production processes as a preliminary test of its suitability for the investigation of the experimental data. Then the relevant cuts[4,14] are introduced into the model via the absorption prescription and the nucleon production processes are reinvestigated. Finally, the model is applied to charge-and strangeness-exchange Λ production and charge-exchange tensor meson production.

1.2 ONE-PARTICLE-INCLUSIVE PROCESSES

Processes of the type $a + b \rightarrow c_1 + c_2 + \ldots + c_n + X$ are called inclusive reactions, where c_i are the n particles observed and X stands for any state which is not observed. This process will be denoted by $(ab, c_1c_2 \ldots c_n)$. For a one-particle-inclusive reaction only one particle in the final state is observed and we have processes of the type $a + b \rightarrow c + X$ (see Fig. 1.1) which will be denoted by (a b,c). The one-particle-inclusive invariant cross section is given by

$$f(ab,c) = (2\pi)^3 \, 2E_c \frac{d^3\sigma}{dp_c^3} = \frac{1}{2\Delta} \sum_{m=1}^{\infty} \left(\prod_z \frac{1}{m_z!} \right) \int \prod_{j=1}^{m} \frac{d^3q_j}{2E_j(2\pi)^3}$$

$$\cdot(2\pi)^4 \, \delta^4(p_n + p_b - p_c - \sum_{j=1}^{m} q_j) \cdot \left| < p_c, q_1 \ldots q_m \mid A \mid p_a, p_b > \right|^2 .$$

In the above equation p_i, i = a,b,c are the momenta of the corresponding particles, $\Sigma\, q_j$ is the momentum of the undetected state X, $\frac{1}{m_z!}$ is the statistical factor for m_z identical particles of type z and $\Delta = \Delta(s, m_a^2, m_b^2)$, with $s = (p_a + p_b)^2$ is defined by

$$\Delta(x, y, z) = (x^2 + y^2 + z^2 - 2xy - 2xz - 2yz).$$

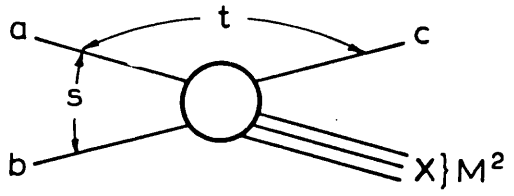

Fig. 1.1. One-particle-inclusive reaction

The invariant cross section depends on three independent variables which are commonly chosen from among

$$s = (p_a + p_b)^2,$$

$$t = (p_a - p_c)^2,$$

$$u = (p_b - p_c)^2,$$

and $M^2 = (p_a + p_b - p_c)^2$. Evidently, these are not independent; we have $s + t + u = M^2 + m_a^2 + m_b^2 + m_c^2$. The choice of variables to be used depends on the physics of the problem. A convenient set for our purposes, to be used in the rest of this text, is s,t and M^2.

The invariant cross section in terms of these invariants will read

$$f(a\,b,c) = (2\pi)^3\, 2\, E_c \frac{d^3\sigma}{dp_c^{\,3}}$$

$$= 16\,\pi^2\,\Delta\,(s,\, m_a^2,\, m_b^2)\,\frac{d^2\sigma}{dM^2 dt}\ \text{(averaged over azimuth)}.$$

The physical region in the M^2-t plane is the Chew-Low plot defined by[15]

$$G\,(s,t,M^2,m_a^2,m_b^2,m_c^2) \leqslant 0,$$

and

$$M^2 \geqslant M^2_{min},$$

where G can be expressed as a determinant

$$G\,(x,y,z,u,v,w) = -\tfrac{1}{2}\begin{vmatrix} 0 & 1 & 1 & 1 & 1 \\ 1 & o & v & x & z \\ 1 & v & 0 & u & y \\ 1 & x & u & 0 & w \\ 1 & z & y & w & 0 \end{vmatrix}.$$

For other properties of G see reference 15.

It was suggested by Mueller[11] that the inclusive cross section for the process a + b → c + X could be related to a discontinuity in the analytically continued forward amplitude for the process a + b + c' → a' + b' + c, where "forward" in this context means the outgoing particles have the same momenta as the incoming ones ($p_a = p_{a'}$, $p_b = p_{b'}$, $p_{c'} = p_c$). However, we have used superscript "'" as indication that they may have different helicity states. This Mueller hypothesis is known as generalized optical theorem and is shown diagramatically in Fig. 1.2.

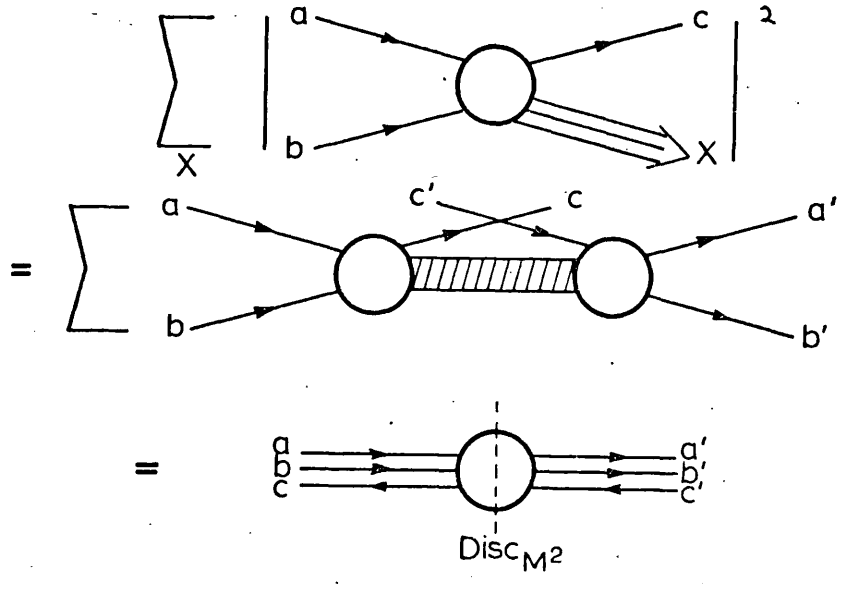

Fig. 1.2. Generalized optical theorem

It has been generally understood that discontinuities of scattering amplitudes arise from the unitarity condition and the formation of various intermediate states. This is, in fact, the basis of the optical theorem. Now let us apply unitarity to the 3-body amplitude. We find that the corresponding total discontinuity is given by several terms, as shown in Fig. 1.3.

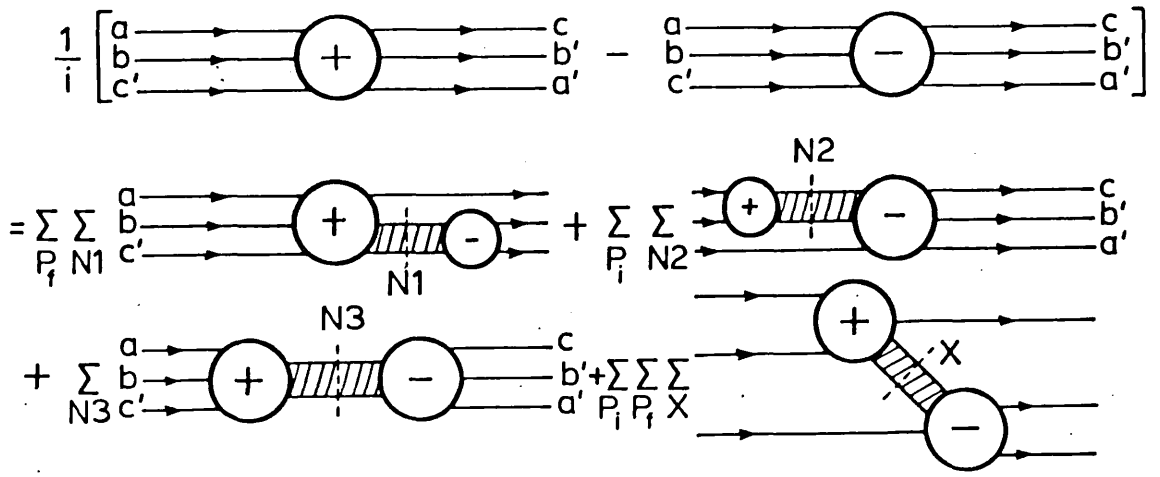

Fig. 1.3. 3-body discontinuity equation

In this discontinuity equation P_i and P_f, respectively, represent permutations of lines for initial-and final-particles, the shaded portions represent the open channel, and an integration over its phase space is implied. A bubble with a "+" refers to an amplitude evaluated in its physical region, and a "-" sign refers to its counter clockwise continuation around the branch point of the energy variables involved. Clearly from Fig. 1.3 one can see that only the last summation on the right hand side resembles the one-particle-inclusive process, and, in fact, one term in this summation corresponds to the process $ab \to cX$, which can be isolated by the special path of continuation in taking the discontinuity. This is illustrated in Fig. 1.4.

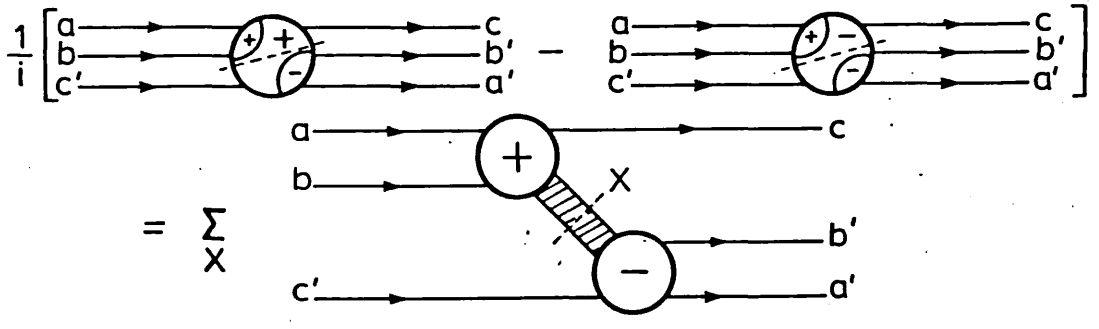

Fig. 1.4. Discontinuity equation (term corresponding to single-particle-inclusive reaction)

the Mueller helicity amplitudes. Kinematical and dynamical properties and limits of one-particle-inclusive processes will be discussed in the following section. The invariant cross section is given by

$$f(ab,c) \sim \sum_{\lambda_a,\lambda_b,\lambda_c} \mathrm{Disc}_{M^2} \langle \lambda_a, \lambda_b, \lambda_c \,|A(s,t,M^2)\,| \lambda_a, \lambda_b, \lambda_c \rangle,$$

and the density matrix element of the finally observed particle is

$$\rho^c_{\lambda_c',\lambda_c} = \frac{\sum_{\lambda_a,\lambda_b} \mathrm{Disc}_{M_2} \langle \lambda_a,\lambda_b,\lambda_c|A(s,t,M^2)|\lambda_a,\lambda_b,\lambda_c' \rangle}{\sum_{\lambda_a,\lambda_b,\lambda_c} \mathrm{Disc}_{M^2} \langle \lambda_a,\lambda_b,\lambda_c|A(s,t,M^2)|\lambda_a,\lambda_b,\lambda_c \rangle}.$$

Similarly, one can define the target and the beam asymmetry[18,20] as

$$A^b_{\lambda_b',\lambda_b} = \frac{\sum_{\lambda_a,\lambda_c} \mathrm{Disc}_{M^2} \langle \lambda_a,\lambda_b',\lambda_c|A(s,t,M^2)|\lambda_a,\lambda_b,\lambda_c \rangle}{\sum_{\lambda_a,\lambda_b,\lambda_c} \mathrm{Disc}_{M^2} \langle \lambda_a,\lambda_b,\lambda_c|A(s,t,M^2)|\lambda_a,\lambda_b,\lambda_c \rangle},$$

and

$$B^a_{\lambda_a',\lambda_a} = \frac{\sum_{\lambda_b,\lambda_c} \mathrm{Disc}_{M^2} \langle \lambda_a',\lambda_b,\lambda_c|A(s,t,M^2)|\lambda_a,\lambda_b,\lambda_c \rangle}{\sum_{\lambda_a,\lambda_b,\lambda_c} \mathrm{Disc}_{M^2} \langle \lambda_a,\lambda_b,\lambda_c|A(s,t,M^2)|\lambda_a,\lambda_b,\lambda_c \rangle},$$

respectively, where we have chosen a as the beam and b as the target particle. Again not all these matrix elements are independent. For example, parity conservation requires that density matrix elements of particle c satisfy

$$\rho^c_{-\lambda_c',-\lambda_c} = (-1)^{\lambda_c'-\lambda_c} \rho^c_{\lambda_c',\lambda_c}.$$

1.3 KINEMATICAL LIMITS AND THE MUELLER-REGGE EXPANSION

The importance of kinematics in evaluating discontinuities has been mentioned before. In this section we will briefly review the kinematical properties[15,21] of one-particle-inclusive processes, their high energy limits[22] and the appropriate Regge analyses of Mueller's theorem in those limits. For this purpose we concentrate on the regions of phase space where the reaction $ab \to cX$, to some extent, is similar to a two-body reaction $ab \to cd$. The similarity and the success of Regge theory in two-body reactions has motivated the extention of Regge analysis to inclusive processes in the above mentioned regions of phase space. But for varying mass of particle X, the analysis is more complicated than that of the two-body case.

We have also mentioned before that the inclusive distribution can be expressed in terms of three independent invariants. However, it is possible to choose any three independent variables, not necessarily invariants, for expressing the inclusive cross section. Let us take p_a, p_b and p_c as the four-momenta for the particles a(beam), b (target) and c, respectively, and M^2 the mass of state X squared. We define the beam and the target fragmentation regions as those subregions of phase space in which particle c looks as if it is a fragment of the beam or target particle and the central region as the rest of phase space. One of the variables is always taken to be the centre-of-mass energy squared of the initial state, s. For the remaining two there is a choice among the following pairs:

i) $(p_{\parallel}, p_{\perp})$, where $p_{\parallel}$ and $p_{\perp}$ are the longitudinal (parallel to the beam p_a) and transverse momentum of particle c. If the centre-of-mass scattering angle is θ then the beam and target fragmentation regions will be reached by letting $\theta \to 0^{\circ}$ and $\theta \to 180^{\circ}$, respectively.

(ii) $(x,p_\perp)$ In this pair, which is good for investigating the fragmentation region, x is the scaled longitudinal momentum, $x \equiv \frac{2p_{||}}{\sqrt{s}}$. The fragmentation region is defined as the region where x and $p_\perp$ are constant and $s \to \infty$. The beam or target fragmentation regions are distinguished by the sign of x which is "+" or "-" , respectively.

(iii) $(y,p_\perp)$, where

$$y = \tfrac{1}{2} \log\left(\frac{E_c+p_{||}}{E_c-p_{||}}\right) = \log\left(\frac{E_c+p_{||}}{m_\perp}\right) = \log\left(\frac{m_\perp}{E_c-p_{||}}\right) \quad ,$$

with the transverse mass $m_\perp \equiv (m_c^2+p_\perp^2)^{\frac{1}{2}}$ and y is the rapidity of particle c. This pair is good for investigating the central region near x = 0.

(iv) (M^2,t), where M^2 and t are both defined before. M^2 is related to x by $\frac{M^2}{s} \simeq 1 - x$ for large s. Since in the c.m. $M^2 = s - 2\sqrt{s}\, E_c + m_c^2$, if $s \gg m_c^2$, then $E_c \simeq p_{||}$ and we have $M^2 \simeq s - 2\sqrt{s}\, p_{||}$. This is the suitable pair for Regge analysis in the beam fragmentation region, while (M^2,u) is the appropriate choice for the study of the target fragmentation region.

At this stage we have crudely defined three regions in phase space and the set of convenient variables for expressing the inclusive distribution in those regions, but have said nothing about how those regions may be reached, how Mueller's theorem can be applied and what sort of Mueller-Regge expansion would be expected. A brief discussion on these subjects follows.

a) Beam fragmentation region

Within this region the following limits are distinguished

i) The single Regge limit; $s \to \infty$, $M^2 \to \infty$, $\frac{s}{M^2}$ and t fixed with the Mueller-Regge expansion shown in Fig. 1.6.

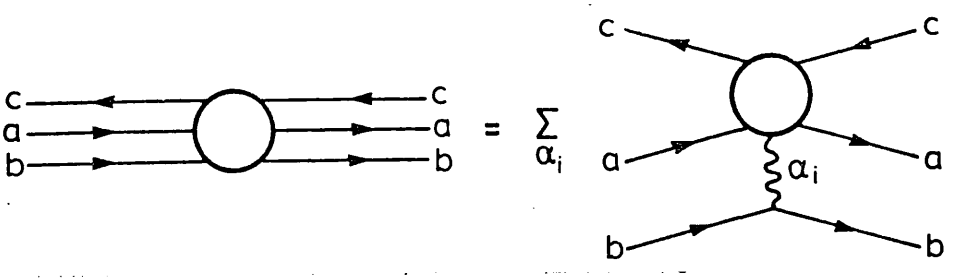

Fig. 1.6. Mueller-Regge expansion for single Regge limit

where $\sum_{\alpha_i}$ denotes sum over all possible Regge exchanges. In this case, the distribution $f(s,t,M^2)$ can be approximated by

$$f(s,t,M^2) \simeq G_p(s,t,M^2) + s^{-\frac{1}{2}} G_M(s,t,M^2),$$

with G_p and G_M, respectively, the scaling and the non-scaling components.

ii) The quasi-two-body limit; $s \to \infty$, M^2 and t fixed with the Mueller-Regge expansion depicted in Fig. 1.7.

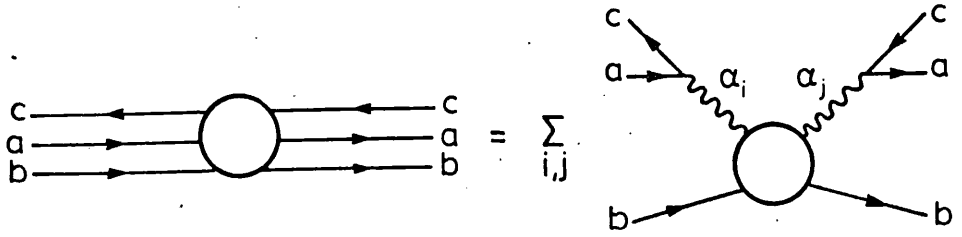

Fig. 1.7. Mueller-Regge expansion for quasi-two-body limit

where $\sum_{ij}$ implies the summation over all possible combinations of i and j Reggeons. The distribution is

$$f(s,t,M^2) = \sum_{ij} \beta_{ij}(t)\, s^{(\alpha_i(t)+\alpha_j(t)-1)}\, T_{ib\to jb}(t,M^2),$$

where $T_{ib\to jb}$ is the forward discontinuity of the Reggeon-particle scattering amplitude. The particle-Reggeon-particle coupling is accounted for by the residue β_{ij}.

iii) The triple-Regge limit; $s \to \infty$, $M^2 \to \infty$, s/M^2 large and t fixed with the Mueller-Regge expansion illustrated in Fig. 1.8.

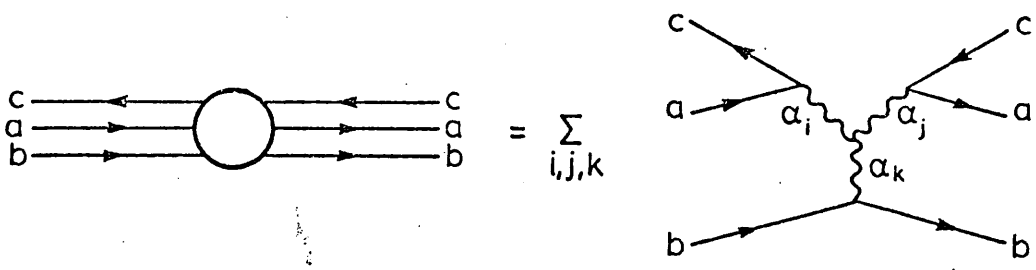

Fig. 1.8. Mueller-Regge expansion for triple-Regge limit

where summation over all possible Reggeons is implied by $\sum_{i,j,k}$. The inclusive cross section is given by[23]

$$f(s,t,M^2) = \sum_{i,j,k} \beta_{ijk}(t)\ (s/M^2)^{(\alpha_i(t)+\alpha_j(t)-\alpha_k(0))}\ s^{(\alpha_k(0)-1)},$$

where β_{ijk} is the total residue.

b) Central region

Double Regge limit; $s \to \infty, |t| \to \infty, |u| \to \infty$ and $m_\perp$ fixed with the Mueller-Regge expansion displayed in Fig. 1.9.

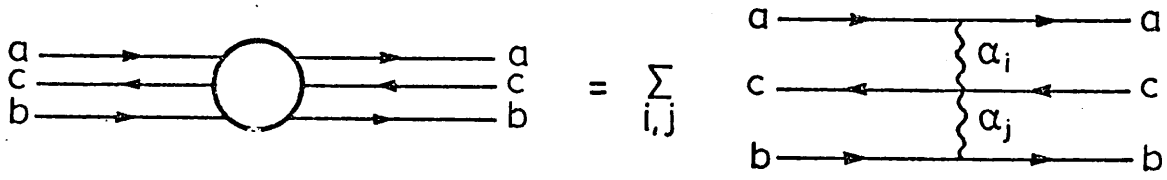

Fig. 1.9. Mueller Regge expansion for central region

where $\sum_{i,j}$ takes into account all possible Regge exchanges. The asymptotic inclusive cross section is given by[24]

$$f(s,t,u) = \sum_{i,j} \beta_{ij}(m_\perp)\ |t|^{\alpha_i(0)-1}\ |u|^{\alpha_j(0)-1}.$$

In this expression all couplings are accounted for by the residue $\beta_{ij}(m_\perp)$.

c) Target fragmentation region

The discussion given for the beam fragmentation region applies to this region as well by changing $t \to u$ and $x \to -x$.

2.2 FORMALISM

The scattering amplitude for the inclusive reaction $ab \to cX$, depicted in Fig. 2.1, for the specific inclusive final state X, is taken to be

$$J_\alpha \, P_{\alpha\beta} \, \Gamma_\beta^X,$$

where J_α is the standard field theoretic current[28,29] at vertex α with all the particles a, c and R put on their mass shell, $P_{\alpha\beta}$ is the Reggeon propagator between vertices α and β and Γ_β^X is the structure function at vertex β. The currents, propagators and structure functions are given for the various processes under investigation as they are needed.

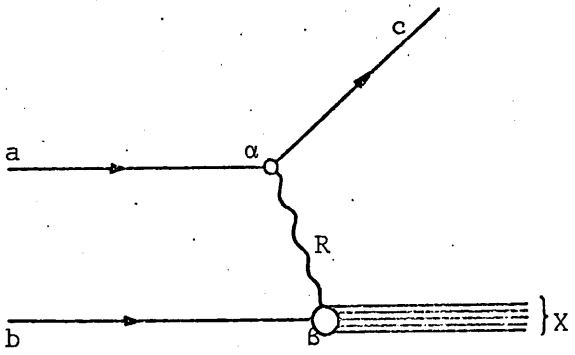

Fig. 2.1. The Born diagram for single-particle-inclusive production in the fragmentation region

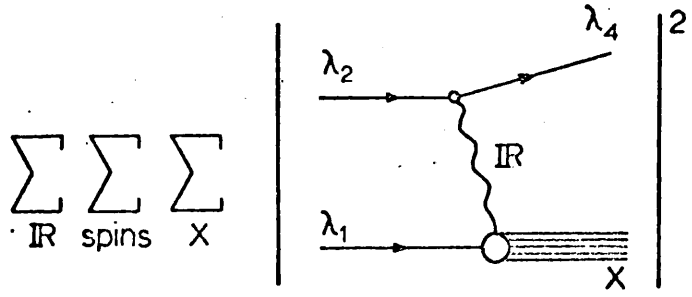

Fig. 2.2. The Mueller-Regge diagram corresponding to Fig. 2.1

In this chapter only nucleon production in nucleon-nucleon scattering, which proceeds by the exchange of a charged non-strange

meson, will be considered, e.g., $pp \to nX$ and $np \to pX$.

The only allowed Regge exchanges for the reactions $pp \to nX$ and $np \to pX$ are the π, the ρ and the A_2. We have assumed strong exchange degeneracy[30] to calculate the A_2 contribution from that of the ρ[31,32].

For π exchange

$$J_\alpha = J_5 = F_M \frac{P^2}{4m_N^2} (\bar{N}\, \gamma_5 N)_{D+2F/3-S},$$

and, for ρ/A_2 exchange we have

$$J_\alpha = J_\mu = \left(\frac{P_\mu}{2m_N} F_C\, (\bar{N}N)_{F+3S} + F_M \frac{1}{4m_N^2} (\bar{N}\, r_\mu N)_{D+2F/3-S}\right),$$

where F_C and F_M are the conventional Sachs from factors[33] and are related to the baryon-baryon-meson coupling, g_{BBM}, by

$$F_C = \left(1 + \frac{Q^2}{2m\mu}\right) g_{BBM},$$

and

$$F_M = \left(1 + \frac{2m}{\mu}\right) g_{BBM},$$

where m and μ are the group theoretic average masses of the baryon and meson, respectively, m_N is the average mass of the incoming and outgoing baryons, $P_\mu = (p_a + p_c)_\mu$ and $Q_\mu = (p_c - p_a)_\mu$, (wherever P^2 and Q^2 appear we will take them to be on-shell, i.e., $P^2 = 2(m_a^2+m_c^2)-\mu^2$ and $Q^2 = \mu^2$), N and $\bar{N}$ are the nucleon and the antinucleon wave functions (see Appendices A and B) and the subscripts D, F and S refer to SU(3) symmetric and antisymmetric octet and singlet couplings, respectively. In the present case the Clebsch-Gordan coefficients corresponding to (D + 2F/3-S) and (F+3S) are $5\sqrt{2}/3$ and $\sqrt{2}$, respectively. In addition

$$r_\mu = \varepsilon_{\mu\nu\kappa\lambda} P^\nu Q^\kappa \gamma^\lambda \gamma^5,$$

and g_{BBM} is calculated from the known pion-nucleon coupling constant[34] by

$$\frac{g^2_{np\pi}}{4\pi} = 30.0 = \frac{g^2}{4\pi} (1 + \frac{2m}{\mu})^2 (1 - \frac{\mu^2}{4m_N^2})^2 (\frac{5\sqrt{2}}{3})^2.$$

The propagators $P_{\alpha\beta}$ have the form

$$\frac{1}{t-m_s^2} \text{ and } \frac{-g_{\mu\nu}+Q_\mu Q_\nu/m_v^2}{t-m_v^2},$$

for pseudoscalar and vector exchange, respectively, with m_s and m_v as the on-shell mass of the exchanged pseudoscalar and vector mesons, respectively. The Reggeization procedure yields

$$\frac{1}{t-m_\pi^2} \to \frac{d\alpha_\pi}{dt}\Big|_{t=m_\pi^2} (-\Gamma(-\alpha_\pi)) \frac{1+\tau_\pi \exp(-i\pi\alpha_\pi)}{2} (\frac{s}{M^2})^{\alpha_\pi},$$

and

$$\frac{1}{t-m_\rho^2} \to \frac{d\alpha_\rho}{dt}\Big|_{t=m_\rho^2} (\Gamma(1-\alpha_\rho)) \frac{1+\tau_\rho \exp(-i\pi\alpha_\rho)}{2} (\frac{s}{M^2})^{\alpha_\rho - 1},$$

where α and τ are the Regge trajectory and signature of the appropriate Reggeon. Our Regge trajectories are taken as

$$\alpha_\pi(t) = 0.013 + 0.650\ t,$$

and

$$\alpha_\rho(t) = 0.470 + 0.905\ t,$$

where these trajectories are derived under the assumption of exchange degeneracy between the pairs of particles π-B and ρ-A_2.

At this stage all we know about the function Γ_β^X is that for pion exchange it must be a pseudoscalar and for ρ/A_2 exchange it

must be a vector.

Since we have assumed that ρ and A_2 are exchange degenerate they do not interfere. Also, it is possible to show that Reggeons of different naturality do not interfere, i.e., there is no interference between the π and the ρ/A_2. Thus, in calculating the differential cross section, as indicated in Fig. 2.2 , we are dealing with the squares of the amplitudes and we have no interference terms. The only things we cannot, in principle, calculate for these amplitudes, at this stage, are the scalar and the tensor quantities

$$\sum_X \Gamma_5^X \Gamma_5^{X\dagger} \text{ and } \sum_X \Gamma_\nu^X \Gamma_{\nu'}^{X\dagger},$$

which arise when we square the amplitudes, sum over X and factorize out the pseudoscalars and vectors that arise from the three-particle vertex (vertex α in Fig. 2.1).

For these quantities we turn to on-shell πp and ρp elastic scattering at $t' = 0$ (see Fig. 2.3). The πp total cross section is related to the transition matrix element $\langle \pi p \mid T \mid \pi p \rangle$ via the standard optical theorem, i.e.

$$D = \text{Disc}_{s'|t'=0} \{ \overline{\sum_{\text{spin}}} \sum_X \langle \pi p \mid T \mid X \rangle \langle X \mid T \mid \pi p \rangle^* \}$$

$$= \text{Flux} \cdot \sigma_{TOT}(\pi p),$$

and similarly for the ρ, where $\overline{\sum_{\text{spin}}}$ indicates an average over the initial and sum over the final p (and ρ in the case of ρp scattering) spins.

previous inclusive data.

Figs. 2.4 and 2.5 display the one-particle-inclusive cross sections for the process ($pn \to pX$), while Fig. 2.7 shows the same quantity for the process ($pp \to nX$). In these figures the theoretical curves, for the unnatural parity, natural parity and total contributions, are shown and compared with the experimental data of FNAL and ISR. The dominance of the unnatural parity exchange contribution, which is completely pion exchange, is evident, with the ratio of the unnatural parity to the natural parity contribution increasing with M^2 for a given s. The M^2 dependence of the data is well accounted for by the model.

In Figs. 2.6 and 2.8 the t dependence of the one-particle-inclusive distributions is shown at fixed M^2. Here it can again be seen that the natural parity contribution, which is due to the exchange of the ρ and the A_2, is overwhelmed by the unnatural parity contribution. The ratio of the unnatural parity to the natural parity contribution decreases with $|t|$. The model gives a forward dip in the t distribution at $t = 0$. The t dependence of the model is compatible with the data although, due to a paucity of the data in t, no conclusive statement can be made.

Because of the higher symmetry scheme, it is easy to extend our model to such processes as $p \overset{A}{\to} \Lambda, \Sigma^o, \Sigma^+, \Sigma^-, \Xi^o, \Xi^+, \Xi^-$ where A is an appropriate hadron. We accomplish this by replacing the π, the ρ and the A_2 trajectories by the K, the $K^*(890)$ and the $K^*(1420)$ trajectories, respectively, and using the appropriate Clebsch-Gordan coefficient at the three particle vertex (vertex α in Fig. 2.1). Reactions of this type would be an interesting test of the model and $pp \to \Lambda X$ will be studied in chapter 4.

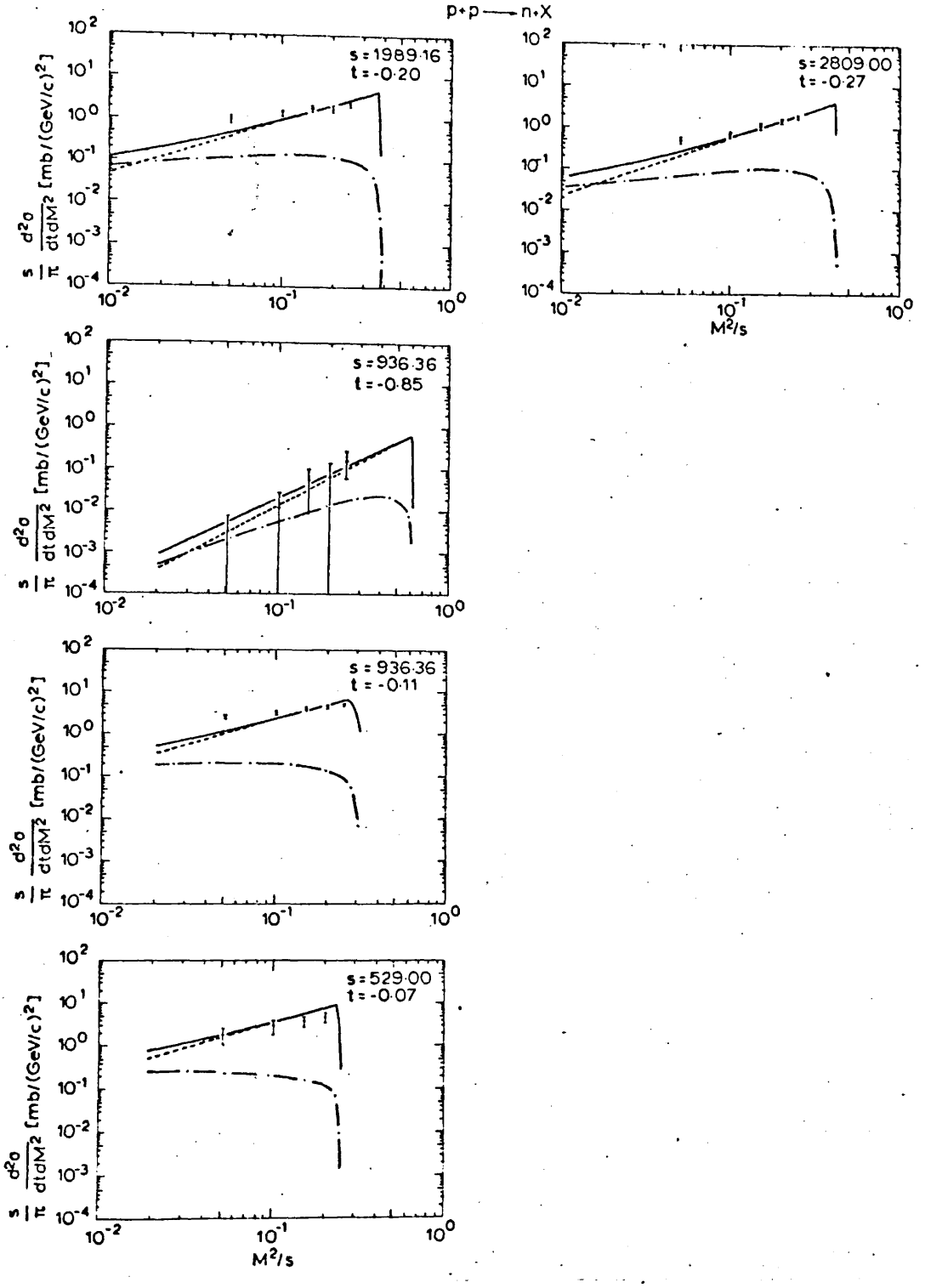

Fig. 2.7 The invariant cross section for ($p \xrightarrow{p} n$) at some ISR energies plotted against M^2/s. Data from ref. 43 (—·—· indicates the natural parity exchange contribution, – – – indicates the unnatural parity exchange contribution, ——— indicates the total exchange contribution)

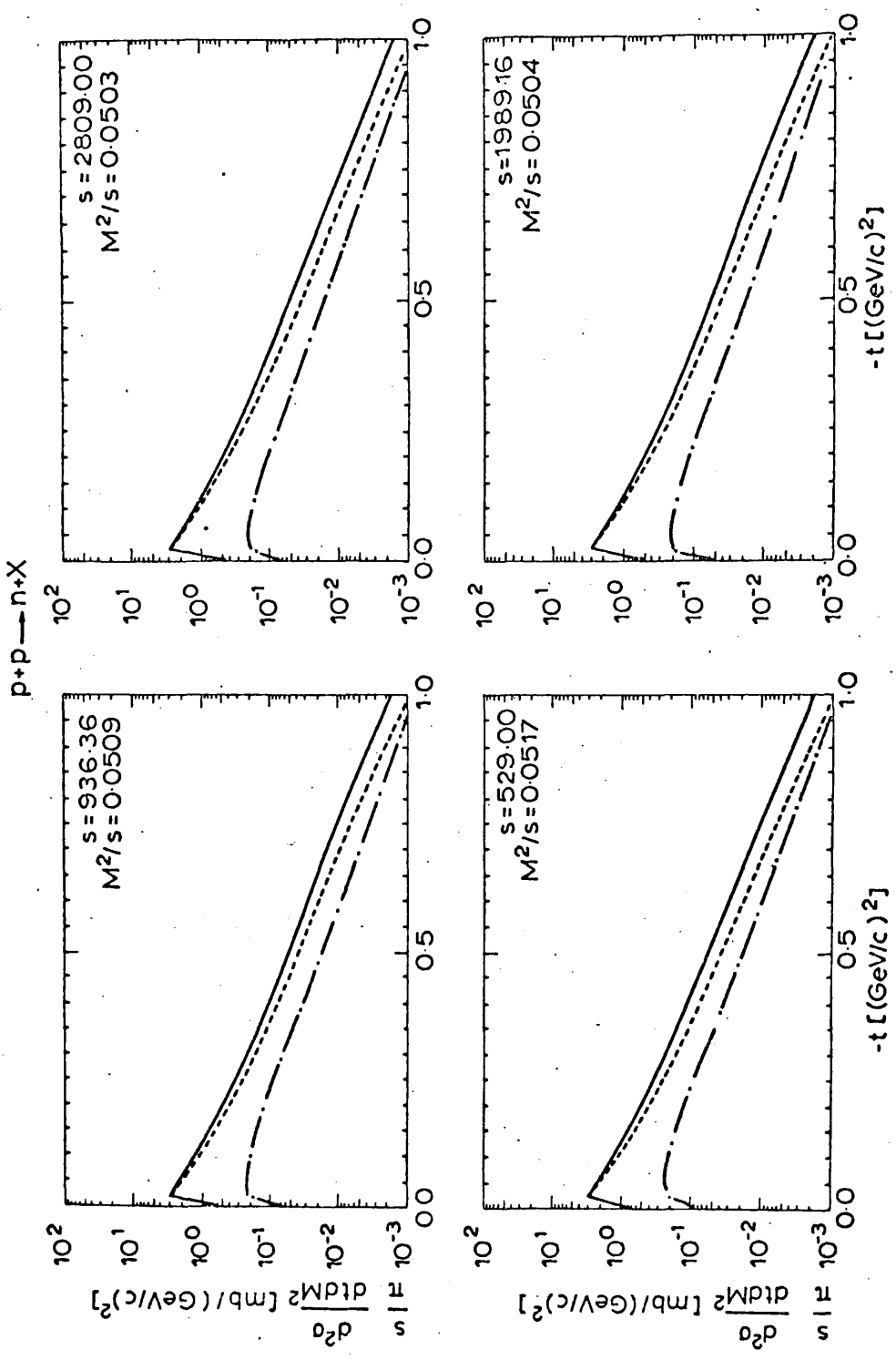

Fig. 2.8 The invariant cross section for ($p \xrightarrow{p} n$) at some ISR energies, plotted against t. (—·—·indicates the natural parity exchange contribution, – – – indicates the unnatural parity exchange contribution, ——— indicates the total exchange contribution)

2.4 CONCLUSION

A Mueller-Regge model has been constructed for studying the one-particle-inclusive processes in the quasi-two-body and triple-Regge limits of the fragmentation region. This parameter-free model, which is the framework of our study of the inclusive reactions, uses the Regge parameters derived from two-body phenomenology.

The model has been applied to the nucleon production processes and shows a surprisingly qualitative success. Nevertheless this qualitative success has no real significance and we have learned from two-body phenomenology to be cautious in interpreting such successes. But this qualitative success encourages us to be more optimistic about accepting this model as the basic framework for more detailed investigations of the inclusive processes and perhaps the explanation of an effectively complete experiment[18].

The model, as it stands, is too naive to give a full description of the inclusive processes. The model has been applied to resonance production processes[41,44]. Obviously these resonances subsequently decay into their more stable products and one would expect any reasonable model to give some sort of explanation of this decay process via the structure in the decay density matrices. This model at the present stage is unable to give any structure for the decay density matrices.

The study of two-body processes has taught us that in any realistic model, which is designed for high energy interactions, apart from pure Regge poles, the inclusion of Regge cuts[45] is essential. Now one might argue that the inadequacy of the model in describing the inclusive processes in a reasonable manner has

P_π and P_ρ, after Reggeization, take the form

$$P_\pi \to \frac{d\alpha_\pi(t)}{dt}\Big|_{t=m_\pi^2} \left(-\Gamma(-\alpha_\pi(t))\right)\left(\frac{1+\tau_\pi \exp(-i\pi\alpha_\pi(t))}{2}\right)\left(\frac{s}{M^2}\right)^{\alpha_\pi(t)},$$

and

$$P_\rho \to \frac{d\alpha_\rho(t)}{dt}\Big|_{t=m_\rho^2} \left(\Gamma(1-\alpha_\rho(t))\right)\left(\frac{1+\tau_\rho \exp(-i\pi\alpha_\rho(t))}{2}\right)\left(\frac{s}{M^2}\right)^{\alpha_\rho(t)-1},$$

respectively, where $\alpha(t) = \alpha_o + \alpha' t$ and τ is the appropriate signature.

Our Regge trajectories are taken as

$$\alpha_\pi(t) = -0.013 + 0.650\ t,$$

and

$$\alpha_\rho(t) = 0.470 + 0.905\ t,$$

where these trajectories are derived under the assumption of exchange degeneracy between the pairs of particles π - B and ρ - A_2.

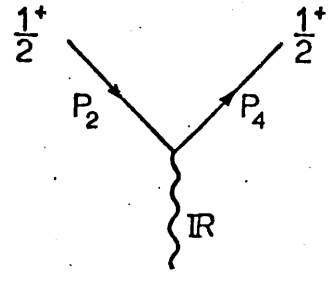

Fig. 3.1 The $(\frac{1}{2}^+, \frac{1}{2}^+, R)$ particle-particle-Reggeon vertex with the momenta appropriately labelled.

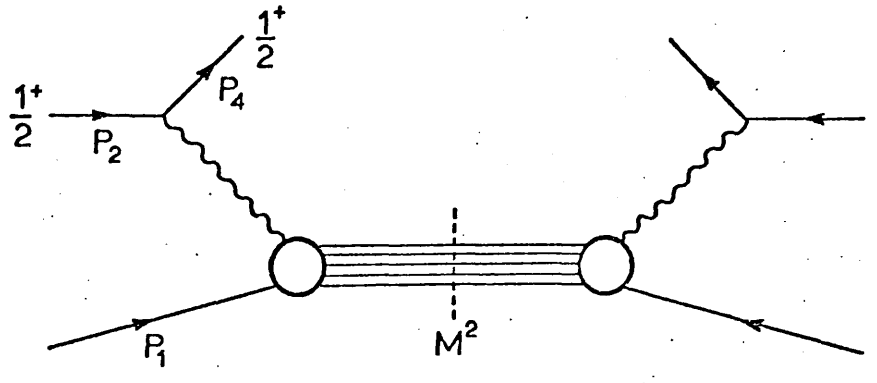

Fig. 3.2 The Mueller-Regge diagram for the inclusive production of $\frac{1}{2}^+$ in the $\frac{1}{2}^+$ beam fragmentation region.

For the πp total cross section we take

$$\sigma_{TOT}(\pi p) = (23.4 + \frac{8.3}{(M^2)^{\frac{1}{2}}})\text{mb},$$

and for the ρp total cross section[37] we take

$$\sigma_{TOT}(\rho p) = 0.270 \frac{0.65}{(1 - t/m_\rho^2)^2} \quad (98.6 + \frac{64.9}{(M^2)^{\frac{1}{2}}}) \text{ mb}.$$

The A_2 contribution was calculated using strong exchange degeneracy, i.e., to get the A_2 exchange contribution from the ρ exchange contribution we simply take $\tau_{A_2} = -\tau_\rho$. A detailed discussion of the calculation of these expressions is given in Chapter 2.

In the Mueller-Regge formalism we sum over all possible helicity states in the final state X. It would be a difficult task to disentangle these to ascertain the precise proportion of helicity flip and helicity non-flip contributions at the inclusive vertex. However, all the Mueller-Regge calculations show strong forward peaking of the inclusive cross section which would suggest the dominance of helicity non-flip contributions at the inclusive vertex. Accordingly, we assume that no net helicity flip takes place at the inclusive vertex. Thus, any net helicity flip arises from the three-particle-vertex.

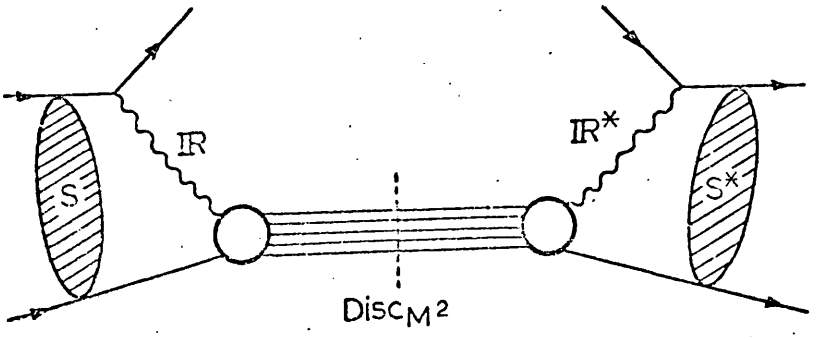

Fig. 3.3 The absorbed Mueller-Regge diagram where elastic scattering in the initial states is taken into account.

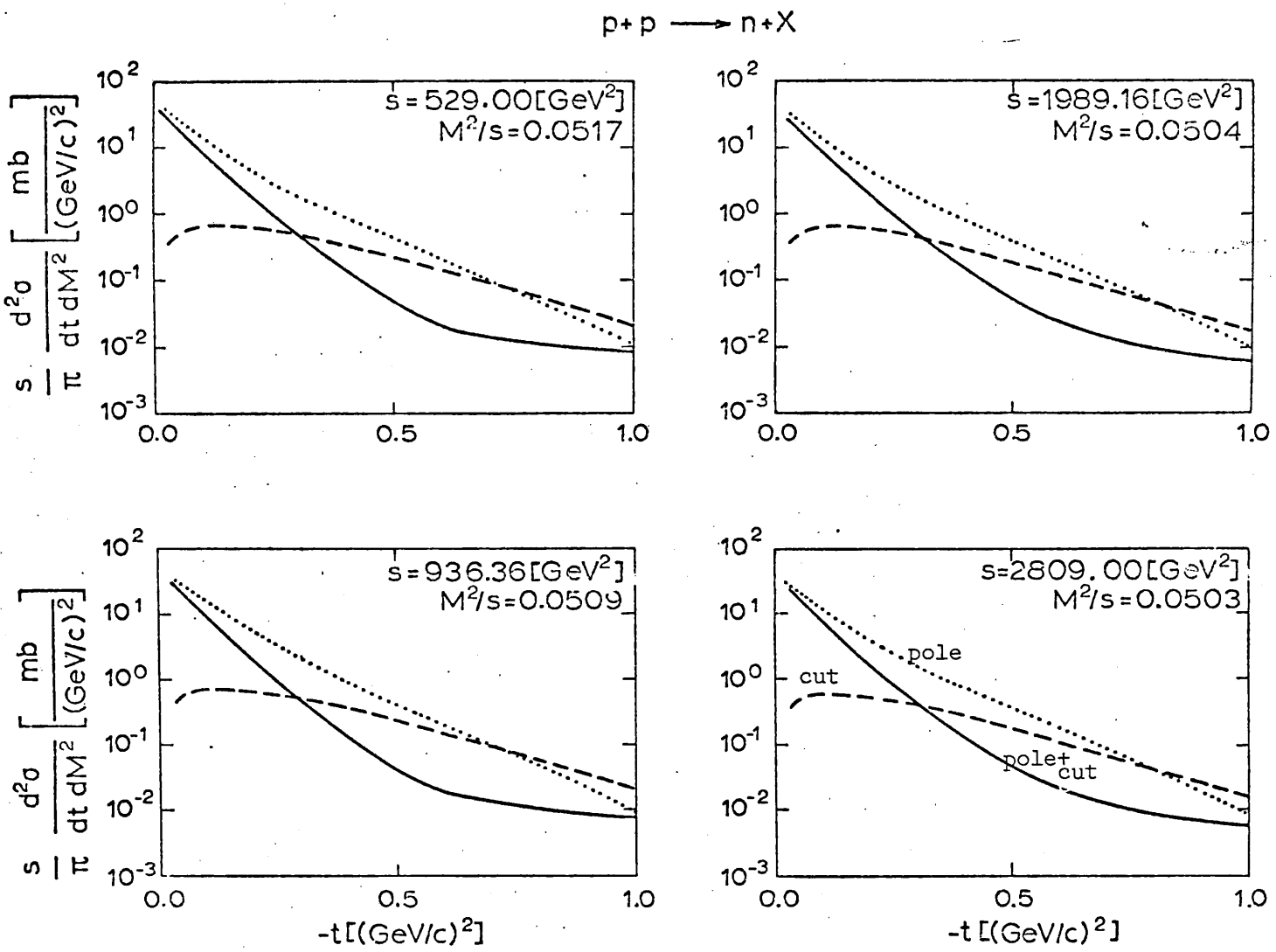

Fig. 3.5 The invariant cross section for (p $\overset{p}{\to}$ n) at some ISR energies plotted against t for fixed M^2/s.

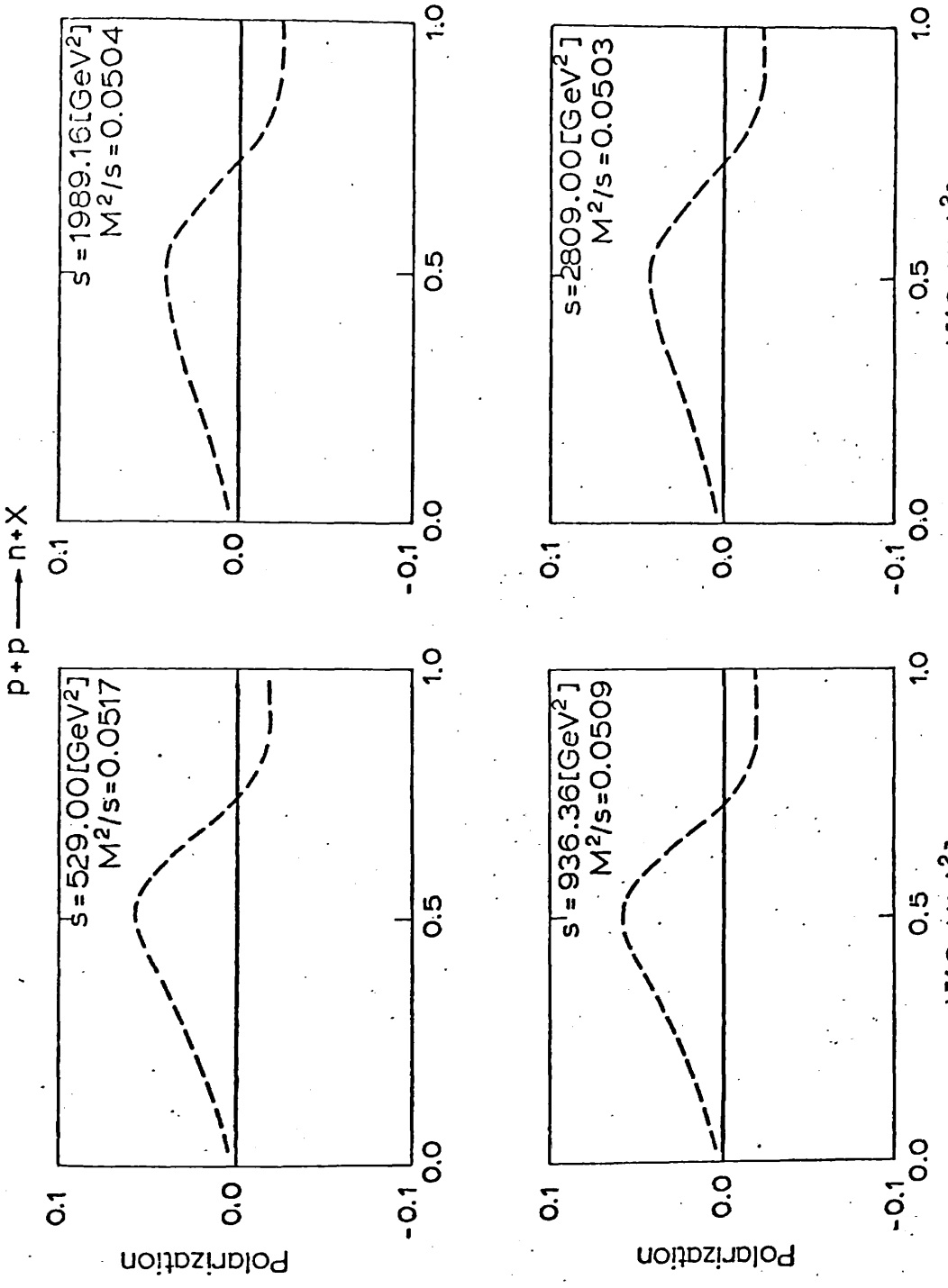

Fig. 3.6 The polarization of the recoil neutron for ($p \xrightarrow{P} n$) at some ISR energies plotted against t for fixed M^2/s.

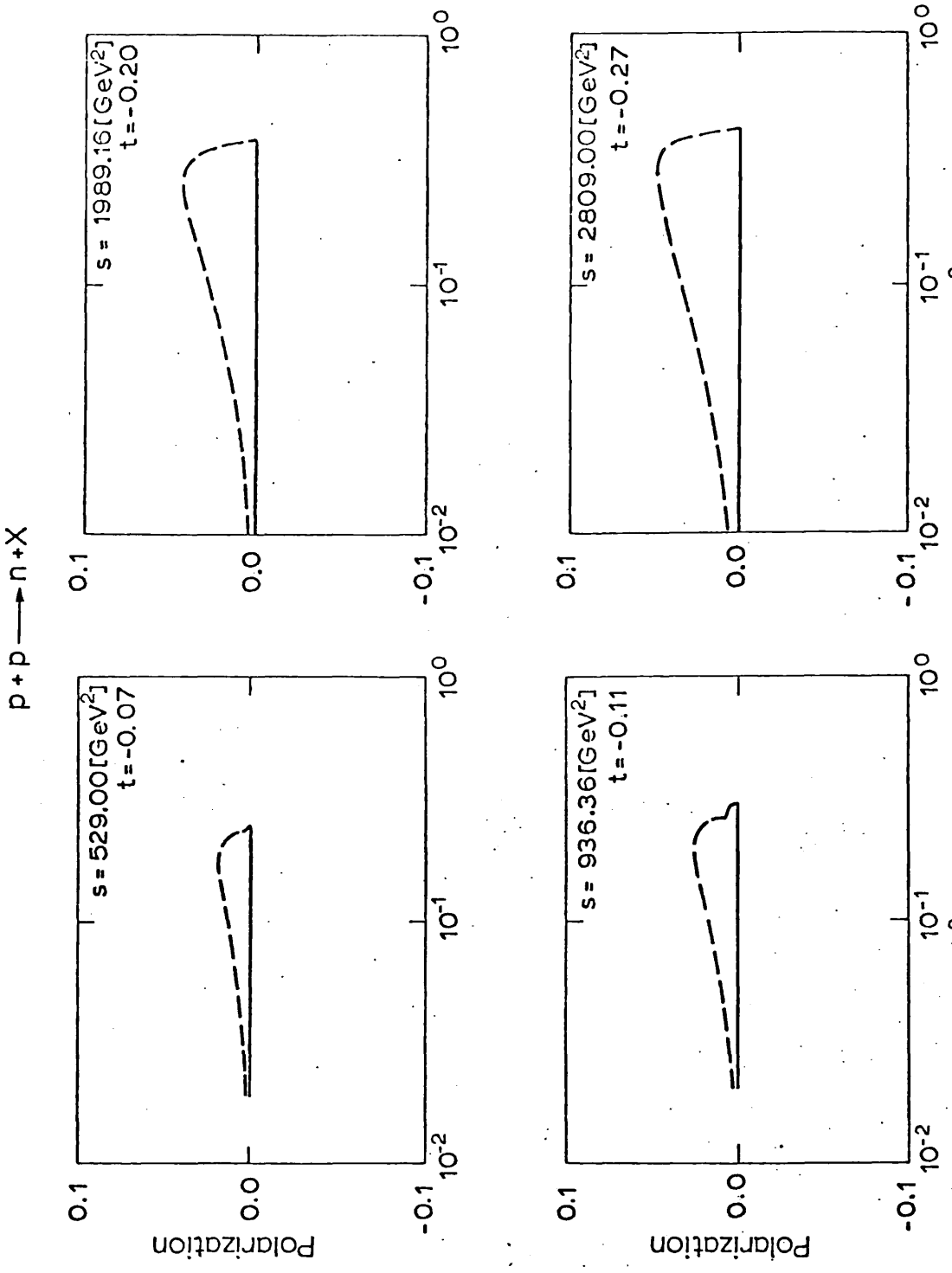

Fig. 3.7 The polarization of the recoil neutron for (p ⃗ n) at some ISR energies plotted against M^2/s for fixed t.

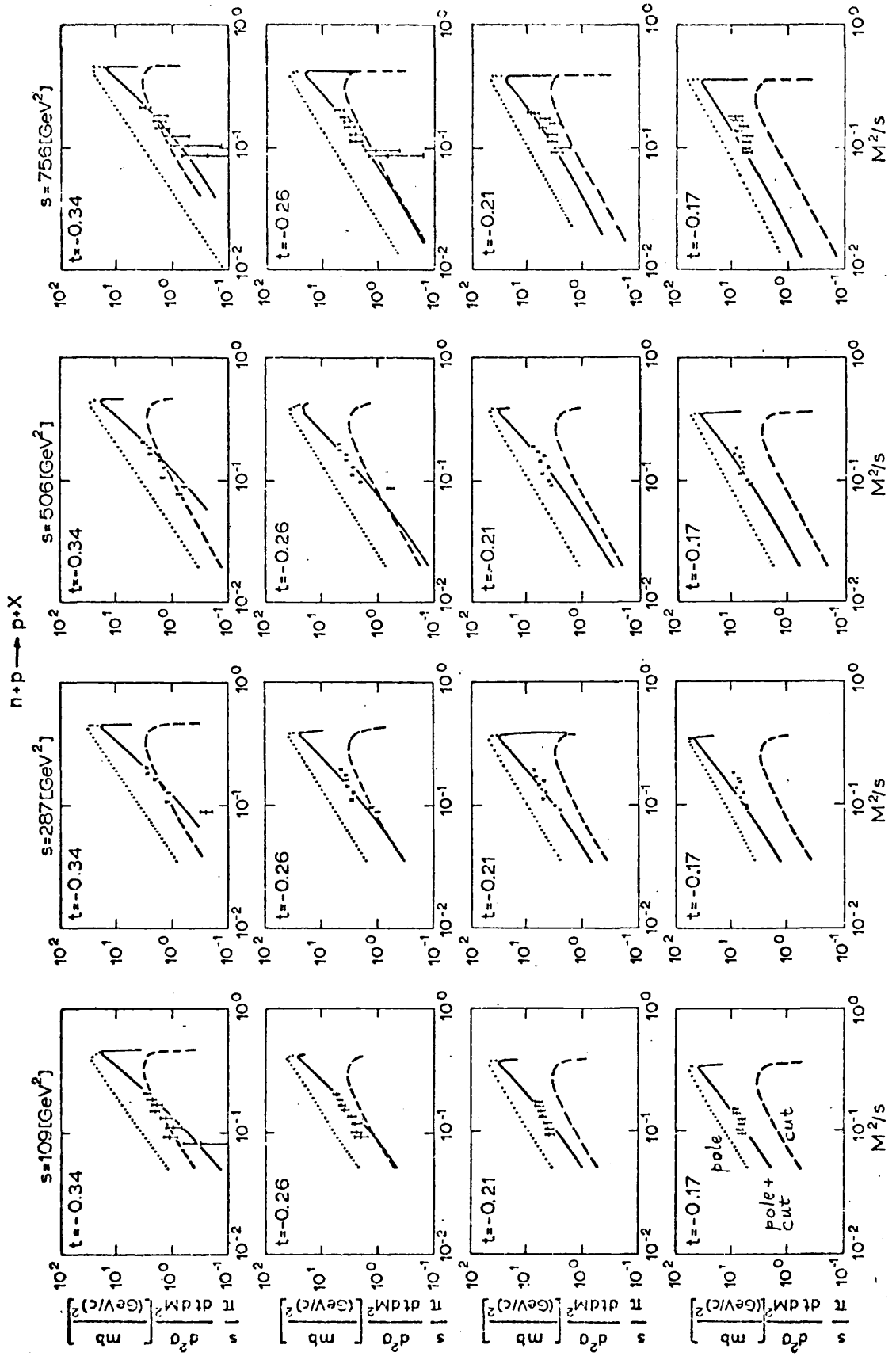

Fig. 3.8 The invariant cross section for ($n \overset{H}{\to} p$) at some FNAL energies plotted against M^2/s for fixed t. Data from Ref. 42.

is evident in this diagram.

In Fig. 3.6 we have plotted the polarization of the recoil neutron as a function of the 4-momentum transfer for fixed M^2/s. Again the scaling behaviour of the amplitudes is clearly manifesting itself. The polarization vanishes at t_{min} by angular momentum conservation, rises to a maximum of about 6% positive polarization at $-t \simeq 0.50$ $(GeV/c)^2$ goes through zero at about $-t \simeq 0.70$ $(GeV/c)^2$ and attains a negative value of about 2%. This behaviour of the polarization is quite dramatic and would be an interesting test of the model.

Fig. 3.7 shows the polarization as a function of M^2/s for fixed momentum transfer. The polarization, as shown in Fig. 3.6 , only reaches appreciable values for large t values.

The predictions of our model are compared in Fig. 3.8 with the date from FNAL[42] on the reaction $(n \overset{p}{\rightarrow} p)$ at four different incident momenta in the range $s = 109$ $(GeV)^2$ to $s = 756$ $(GeV)^2$. This data is of much higher quality than the ISR data shown previously and, as such, provides a much more stringent test of our model calculations. We observe that the s, t and M^2/s dependences of the theoretical distributions are consistent with the data. The modified Mueller-Regge pole amplitudes can be seen to interpolate the experimental data and represents a tru ly remarkable parameter-free fit to the data while the unmodified amplitudes overestimate the experimental data by factors of about 3. Thus, we see that our conjecture that absorptive cut corrections could remedy the normalization problem for the invariant cross section is correct. This provides yet another stimulus to studying cut corrections to the Mueller-Regge model with simple poles, in addition to those already mentioned in the introduction.

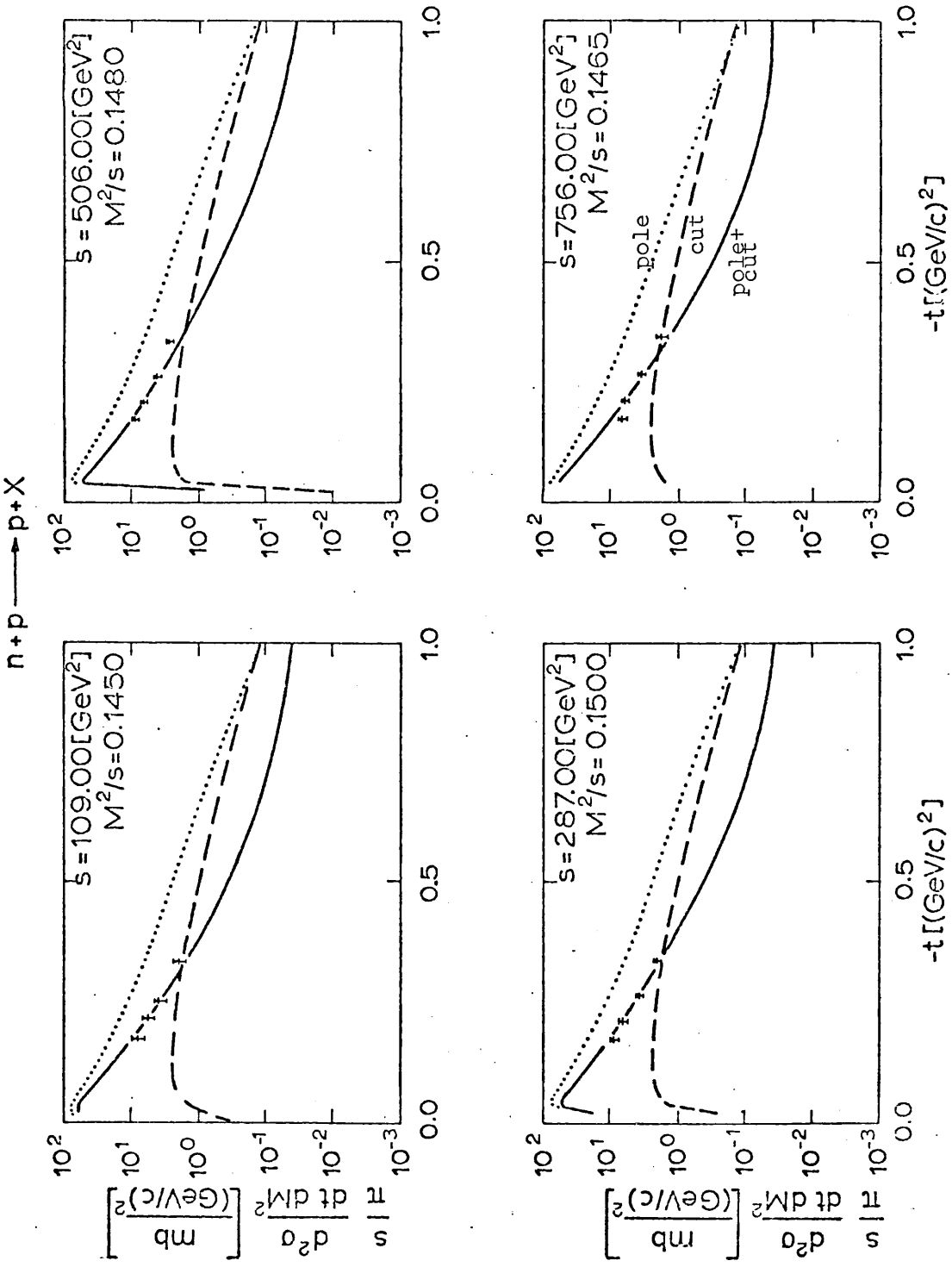

Fig. 3.9 The invariant cross section for (n $\rightarrow$ p) at some FNAL energies plotted against t for fixed M^2/s. Data from Ref. 42.

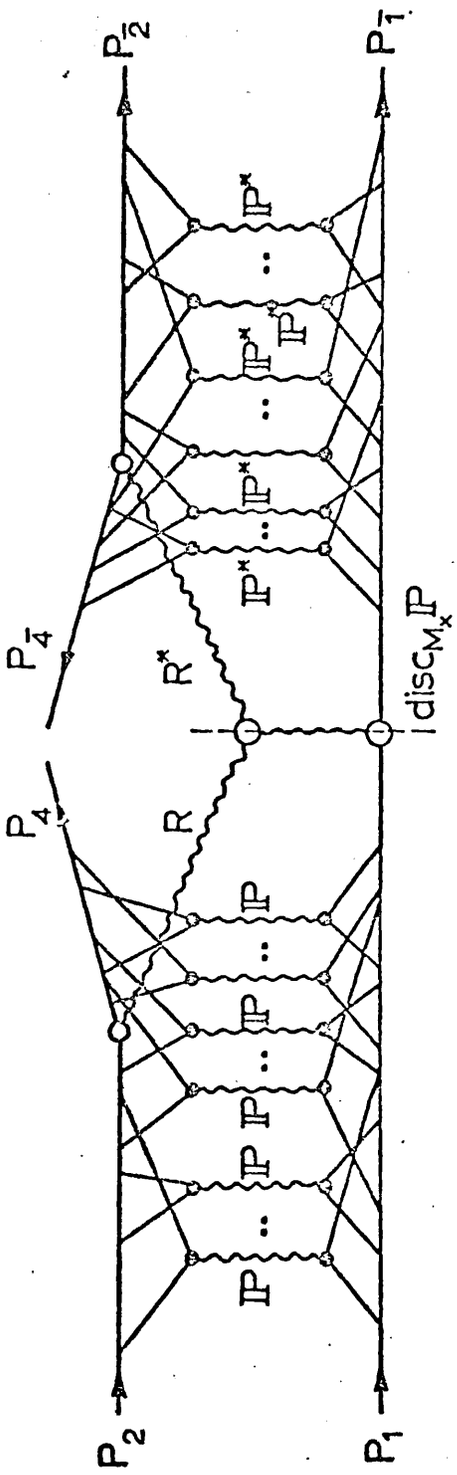

Fig. 3.13 The sum of all Pomeron-induced rescattering corrections to the Mueller-Regge Y graph for the inclusive production of a nucleon.

It was shown[59] that the closed expression for a Regge eikonal formula for summing all Pomeron exchange rescattering corrections to the Mueller-Regge Y graph shown in Fig. 3.13 is given by

$$H(s,t,M^2) = \int \frac{d^2\vec{Q}_2}{(2\pi)^2} \frac{d^2\vec{Q}_4}{(2\pi)^2} \frac{d^2\vec{Q}_2}{(2\pi)^2} \frac{d^2\vec{Q}_4}{(2\pi)^2}$$

$$\cdot S(\vec{Q}_2,\vec{Q}_4)Y(t_{24},\vec{t}_{24},t_o,s,M^2)\bar{S}(\vec{Q}_2,\vec{Q}_4),$$

where

$$S(\vec{Q}_2,\vec{Q}_4) = \int d^2\vec{B}_{21} d^2\vec{B}_{41}\, e^{i\vec{Q}_2\cdot\vec{B}_{21} + i\vec{Q}_3\cdot\vec{B}_{41}}$$

$$\cdot e^{i\chi_{21}(B_{21}) + i\chi_{24,1}(B_{21},B_{41}) + i\chi_{41}(B_{41})},$$

and

$$\bar{S}(\vec{Q}_2,\vec{Q}_4) = \int d^2\vec{B}_{21}\, d^2\vec{B}_{41}\, e^{-i\vec{Q}_2\cdot\vec{B}_{21} - i\vec{Q}_4\vec{B}_{41}}$$

$$\cdot e^{i\chi^*_{21}(B_{21}) - i\chi_{24,1}(B_{21},B_{41}) - i\chi_{41}(B_{41})},$$

where the variables are defined in Ref. 59 and χ_{21}, χ_{41} and $\chi_{24,1}$ are eikonal phases between the indicated particles.

Calculations using this model are presently being carried out[60]. Although these calculations should agree, to leading order, with the calculations presented here it will be interesting to see if any strong M^2/s dependence results from the inclusion of the eikonal phases χ_{41} and $\chi_{24,1}$. In addition, it will be interesting to observe any changes in the predicted nucleon polarization.

CHAPTER FOUR

Λ POLARIZATION

The evidence for including Regge cut corrections to the Mueller-Regge model for inclusive processes of the form a + b → c + X in the triple-Regge region, both from theoretical[52,61] and phenomenological[36,48-51] considerations, is persuasive. The reaction p + p → Λ + X, where the polarization of the Λ is observed, provides a nice test of any particular method for including Regge cuts in a Mueller-Regge model. This is because in a Mueller-Regge model with simple poles the Λ polarization is identically zero. The Polarization results from Regge cut contributions and thus provides a sensitive measure of their strength and functional forms.

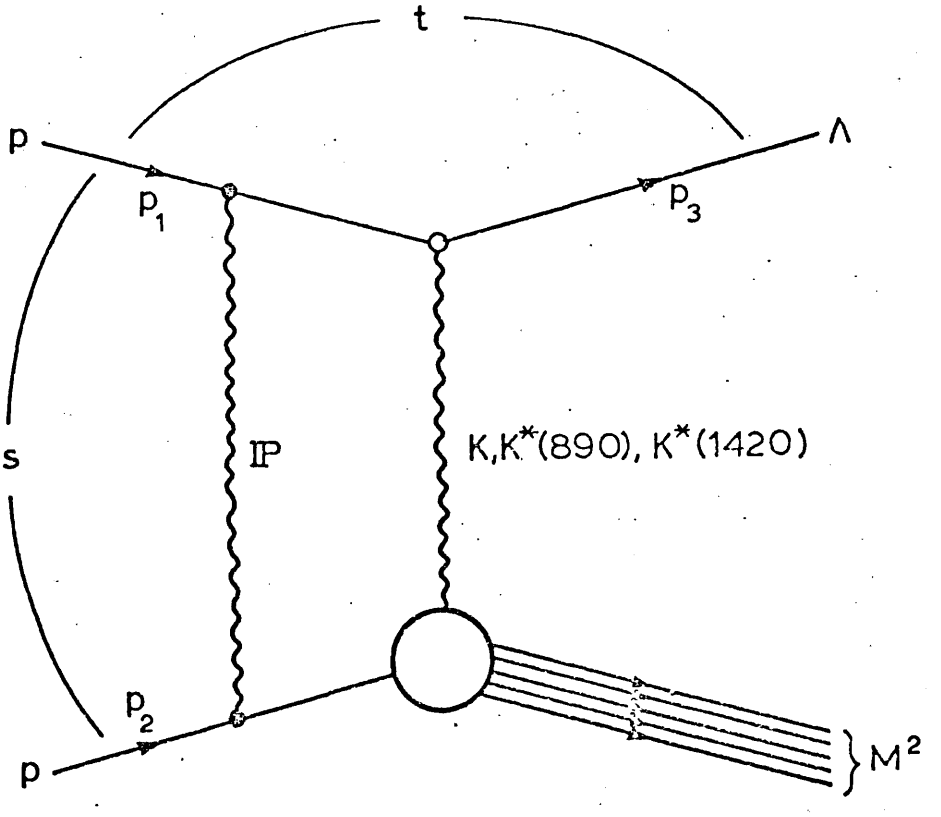

Fig. 4.1 The single-particle-inclusive diagram for p + p → Λ + X with absorption corrections in the initial state. The particles, the four-momenta and the Mandelstam variables are indicated.

For the process $p + p \to \Lambda + X$ the couplings to the three-particle vertices as shown in Fig. 4.1 are given by

$$\phi_K(s,t,M^2) = g_{p\Lambda K}(\bar{N}\gamma_5 N)P_K\Gamma_K^X,$$

and

$$\phi_{K^*}(s,t,M^2) = \left[M_1(t)\frac{P_\mu}{2m_N}(\bar{N}N) + M_2(t)\bar{N}\gamma_\mu N \right] (p_1)^\mu P_{K^*}\Gamma_{K^*}^X,$$

for K and K*(890) exchange, respectively. Here s and t are the usual Mandelstam variables defined by (see Fig. 4.1) $s = (p_1 + p_2)^2$ and $t = (p_3 - p_1)^2$, M is the missing mass, $g^2_{p\Lambda K}/4\pi$ is taken as 16., m_N is the nucleon mass, $M_1(t)$ and $M_2(t)$ are form factors related to the conventional Sachs form factors[33] F_C and F_M by the relations

$$M_1 = F_C - F_M \text{ and } M_2 = \left(1 + \frac{t}{4m_N^2}\right) F_M,$$

$P_\mu = (p_3 + p_1)_\mu$ and N and $\bar{N}$ are the wave functions of spin $\frac{1}{2}$ particle and antiparticles, respectively. The structure functions Γ_K^X and $\Gamma_{K^*}^X$ are defined by

$$\Gamma_K^X = \sqrt{2\Delta(M^2,m_K^2,m_p^2)\sigma_{TOT}(Kp)} \text{ and } \Gamma_{K^*}^X = \sqrt{\frac{8m_{K^*}^2\sigma_{TOT}(K^*p)}{\Delta(M^2,m_{K^*}^2,m_p^2)}},$$

respectively, where m_K and m_{K^*} are the masses of the K and the K*(890) mesons, respectively, m_p is the proton mass and

$$\Delta(x,y,z) = (x^2 + y^2 + z^2 - 2xy - 2xz - 2yz) .$$

The variable $P_\perp$ is given by $P_\perp = q\sin\theta$. The propagators P_K and P_{K^*}, after Reggeization, take the form

$$P_K \to \frac{d\alpha_K(t)}{dt}\Bigg|_{t = m_K^2} \left[-\Gamma(-\alpha_K(t)) \right] \frac{1+\tau_K \exp\left[-i\pi\alpha_K(t)\right]}{2} \left[\frac{s}{M^2}\right]^{\alpha_K(t)},$$

and

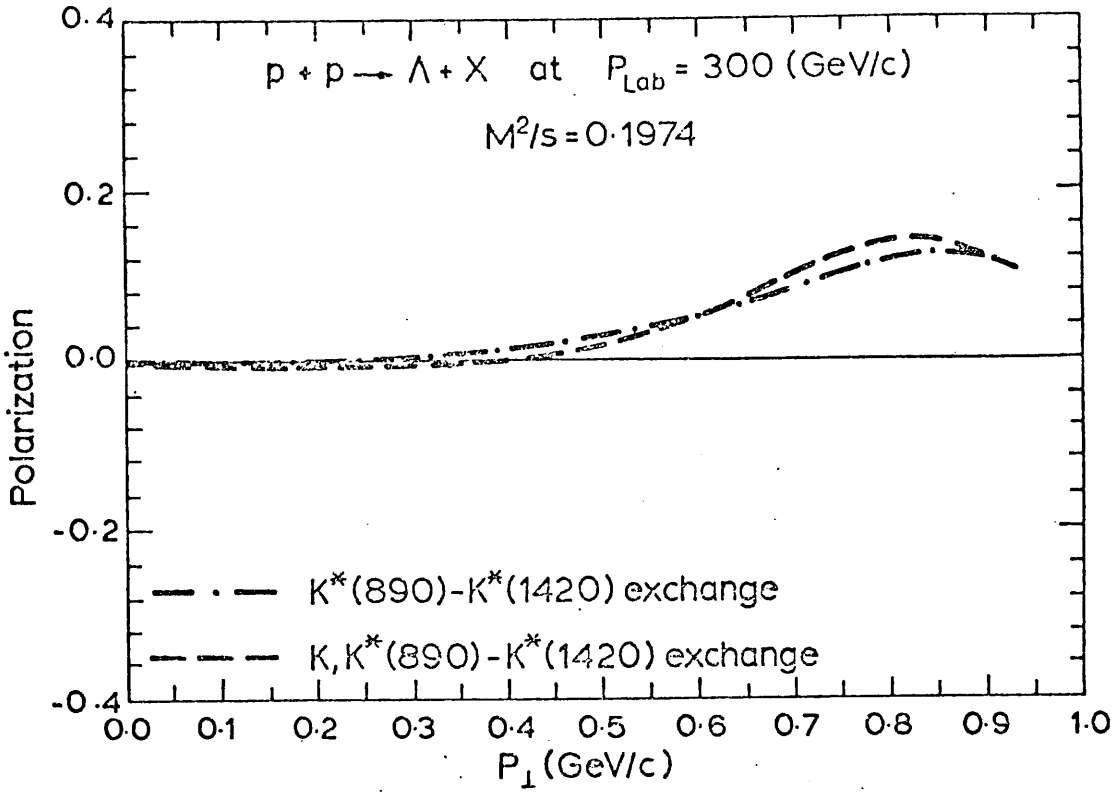

Fig. 4.2 The Λ polarization for ($p \xrightarrow{p} \Lambda$) at $M^2/s = 0.1974$ showing the contributions for $K^*(890) - K^*(1420)$ and $K, K^*(890) - K^*(1420)$ exchanges.

In Figs. 4.2, 4.3 we show the results of our calculations for the Λ polarization in the reaction $p + p \to \Lambda + X$ at 300 (GeV/c) for two different values of the variables M^2/s. At $M^2/s = 0.1974$ (see Fig. 4.2) we see that when the K*(890) - K*(1420) exchange degenerate trajectory is exchanged the polarization is small and positive for $0 < P_\perp < 0.8$ (GeV/c). However, the exchange of the K, K*(890) - K*(1420) leads to a polarization which is small and negative for $P_\perp < 0.38$ (GeV/c) with our choice of parameters. In Fig. 4.3 we have plotted our result for $M^2/s = 0.0115$. Here the K*(890) - K*(1420) exchange dominates the K exchange in any case. As $M^2 \to 0$ we find no difference between the results from K*(890)-K*(1420) exchange and the results for K, K*(890) - K*(1420) exchange. Of course our model calculations of the Λ polarization scale. The Basel convention is adopted for our definition of the polarization vector.

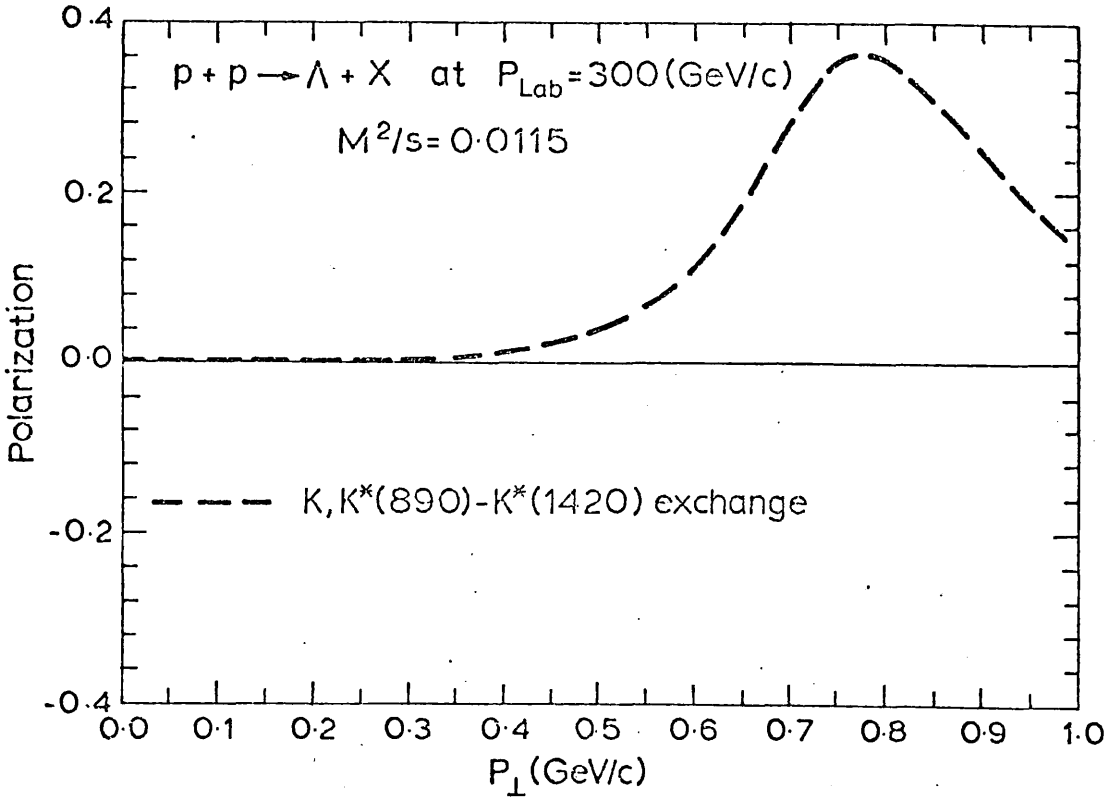

Fig. 4.3 The Λ polarization for ($p \xrightarrow{p} \Lambda$) at $M^2/s = 0.0115$ resulting from K, $K^*(890)$ - $K^*(1420)$ exchange.

Because the experimental data is independent of the target it seems worthwhile to compare the data on the Λ polarization in p + Be → Λ + X with our model calculations on p + p → Λ + X. This should, at least, give us the sign and the order of magnitude of the Λ polarization we would expect to observe in p + p → Λ + X. However, our model is a triple-Regge model and should only be applicable in the triple-Regge region of phase space. The experimental data exists outside of the triple-Regge region, e.g. for $M^2/s = 0.31$. But the data is independent of x so we do not introduce too much error by comparing our triple-Regge model calculation with data accumulated outside the triple-Regge region.

In Fig. 4.4 we see the results of our model calculations for both K*(890) - K*(1420) and K, K*(890) - K*(1420) exchanges for the Λ polarization for $p + p \rightarrow \Lambda + X$ compared with the data for $p + Be \rightarrow \Lambda + X$. The data is positive and small for $P_\perp < 0.8$ (GeV/c) and seems to agree quite well with the result of K*(890) - K*(1420) exchange. Keeping Fig. 4.3 in mind we can see that in the triple-Regge region all the exchanges will lead to positive Λ polarization as is observed experimentally. It should be pointed out that both the sign and the magnitude of the Λ polarization given by our model calculation are predictions of the model resulting from our absorption corrections and are not arbitrary.

It is now well established that polarization effects exist in single-particle-inclusive reactions. These polarization effects can be treated with absorption correction models[48-51], and this leads to sensible results. Because of its simplicity it would be most useful to have experimental data on the Λ polarization for the reaction $p + p \rightarrow \Lambda + X$ in the triple-Regge region itself. The data which is presently available on the reactions $p + Be(Cu) \rightarrow \Lambda + X$ certainly indicates that the Λ polarization will be small and positive. Polarization of the Λ in the interesting process $pp \rightarrow \Lambda X$ was also studied by Paige and Sidhu[52] within an absorptive model, by Turbiner[66] in Reggeized one-pion-exchange model, by Owens[20,67] and by Chang et al. in a diffractive excitation model[68].

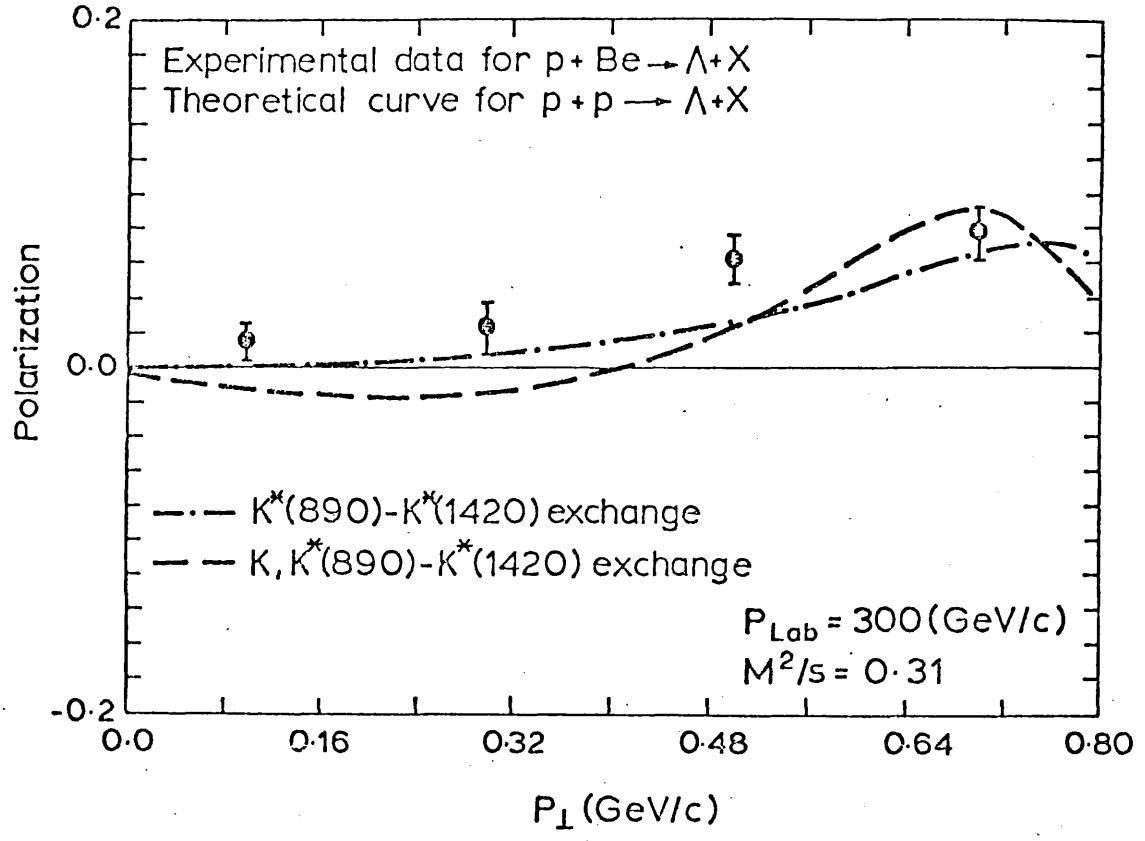

Fig. 4.4 The polarization for ($p \xrightarrow{p} \Lambda$) at $M^2/s = 0.31$ compared with the experimental Λ polarization for ($p \xrightarrow{Be} \Lambda$) showing the various exchange contributions.

$$\sigma_{TOT}(\pi p) = (23.4 + \frac{8.3}{(M^2)^{\frac{1}{2}}})\ \text{mb}.$$

The elastic rescattering effect in the initial state, shown in Fig. 5.1, is taken into account through absorption in impact parameter space. The corrected amplitudes are of the form

$$H_{abs}^{\lambda_c\lambda_c'} = S^*_{a'b'}(b_2)\, H^{\lambda_c\lambda_c'}(b_2,b_1)\, S_{ab}(b_1),$$

where S(b) is the elastic scattering S-matrix. Assuming that the elastic rescattering effects in the ab and the $\bar{c}b$ channels are approximately equal, we have made the replacement

$$S^{\frac{1}{2}}_{ab}(b)\, S^{\frac{1}{2}}_{\bar{c}b}(b) \simeq \frac{S_{ab}(b)+S_{\bar{c}b}(b)}{2} \simeq 1 - C\exp(-\lambda b^2) = S(b),$$

where b is the impact parameter, C is the opacity, $\lambda = R^{-2}$ where R is the target interaction radius. We take C = 0.70 and $\lambda = 0.068$ $(\text{GeV/c})^2$. The corrected Mueller-Regge amplitudes are given by

$$H_{abs}^{\lambda_c\lambda_c'}(s,\tau,M^2) = \int_0^\infty \tau_1 d\tau_1 \int_0^\infty \tau_2 d\tau_2 \int_0^\infty b_1 db_1\, J_\nu(b_1\tau) J_\nu(b_1\tau_1)\, S(b_1)$$

$$\cdot \int_0^\infty b_2 db_2\, J_{\nu'}(b_2\tau)\, J_{\nu'}(b_2\tau_2)\, H^{\lambda_c\lambda_c'}(s,\tau_1,\tau_2,M^2)\, S^*(b_2),$$

which, after performing the integration over impact parameter, reduces to

$$H_{abs}^{\lambda_c\lambda_c'}(s,\tau,M^2) = \int_0^\infty \tau_1 d\tau_1 \int_0^\infty \tau_2 d\tau_2 \left[\frac{1}{\tau}\delta(\tau-\tau_1) - \frac{C}{2\lambda}\exp\{-\frac{[\tau^2+\tau_1^2]}{4\lambda}\} I_\nu(\frac{\tau\tau_1}{2\lambda})\right]$$

$$\cdot H^{\lambda_c\lambda_c'}(s,\tau_1,\tau_2,M^2)\left[\frac{1}{\tau}\delta(\tau-\tau_2) - \frac{C}{2\lambda}\exp\{-\frac{[\tau^2+\tau_2^2]}{4\lambda}\} I_{\nu'}(\frac{\tau\tau_2}{2\lambda})\right].$$

In this equation, using the simplifying assumption that the inclusive vertex is dominated by helicity non-flip*, ν and ν' will take

*Following the formalism of Ref.(50) as given by equation (2.13) we can relax this assumption and sum over all the spins of the inclusive cluster. For small t the results of our calculation remain unaltered.

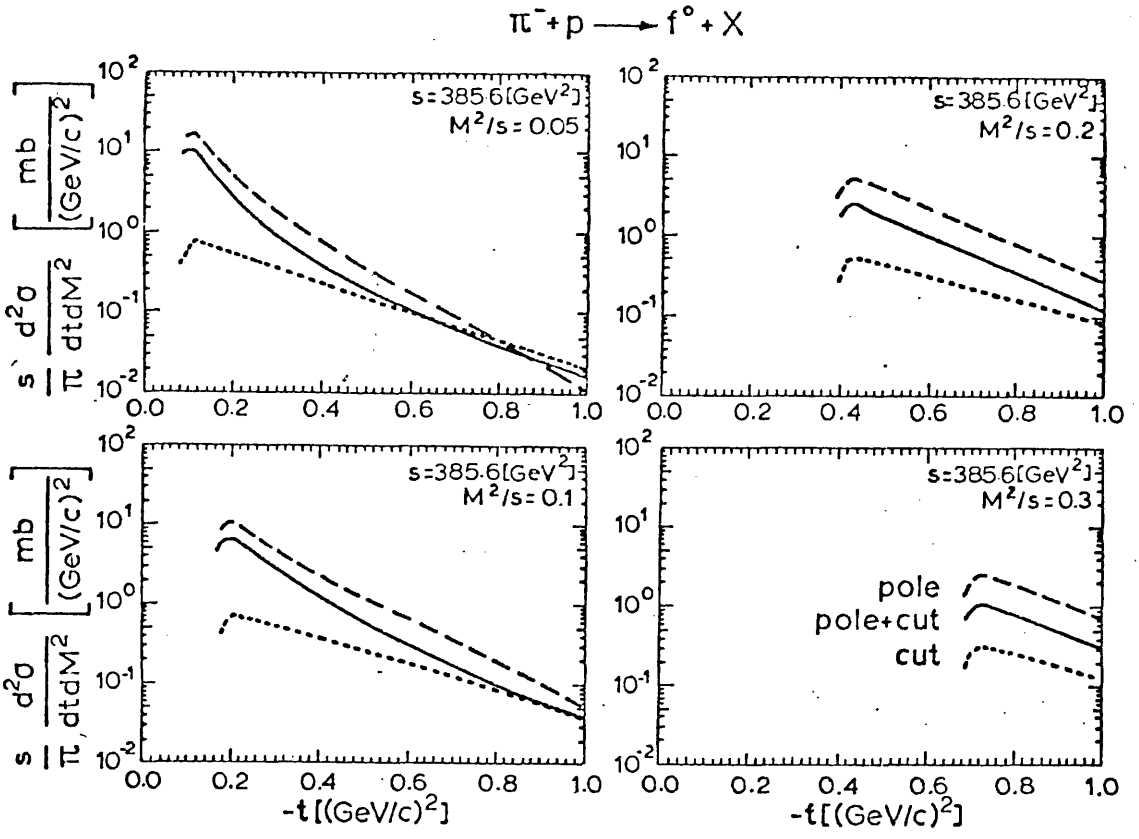

Fig. 5.2 The invariant differential cross sections for fixed M^2/s.

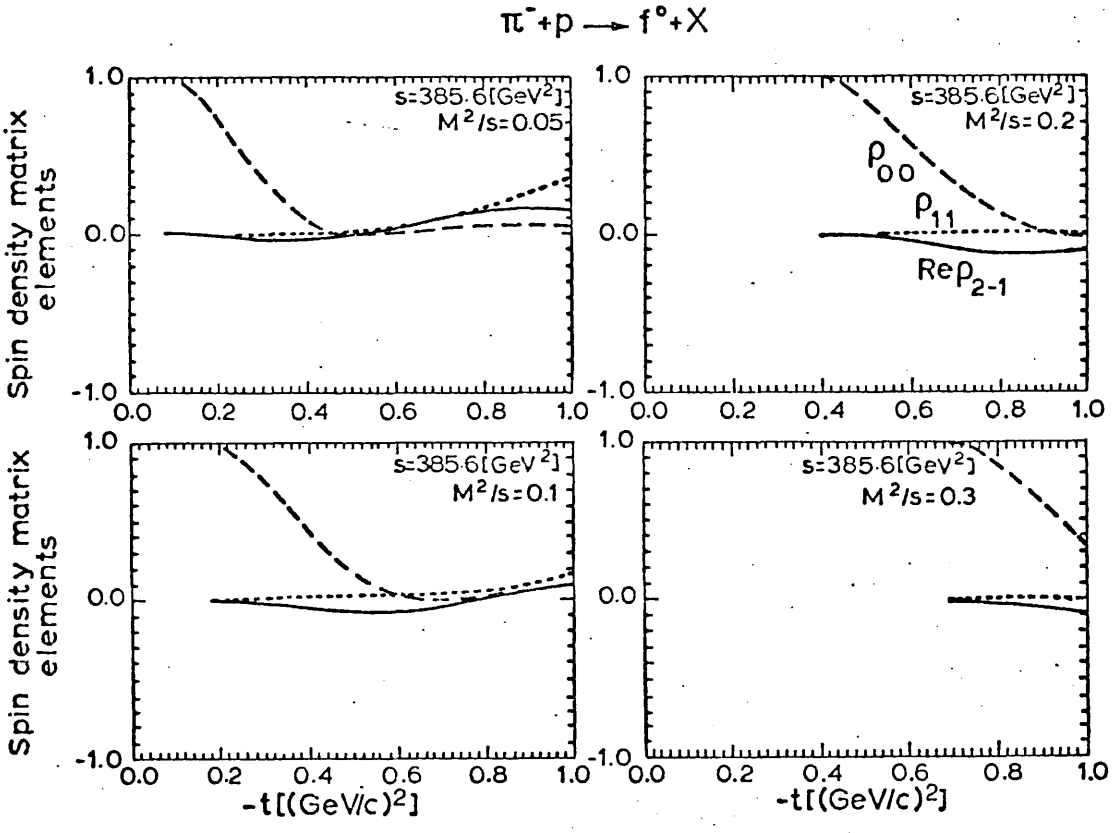

Fig. 5.3 The decay density matrix elements for fixed M^2/s.

found that $\mathrm{Re}\rho_{21}$ is generally small with no dependence on t or M^2/s and that $\mathrm{Re}\rho_{20}$ is negative and changes little with variation in t or M^2/s. Because of this, we only plot the decay density matrix elements ρ_{00}, ρ_{11} and Re ρ_{2-1}.

All the calculations of differential cross sections and density matrix elements were carried out numerically[64]. All the figures were, for accuracy, plotted by computer[56].

The turnover in the differential cross section (see Figs. 5.2 and 5.4) is expected because near the edge of phase space the power dependence on t dominates over the exponential dependence on t. The expressions for $H^{\lambda_c\lambda_c}_{abs}$ for $\lambda_c = \pm 2$ and ± 1 depend, respectively, on $\sin^2\theta$ and $\sin\theta$ which vanish at $t = t_{min}$. Because H^{00}_{abs} is falling rapidly for t near t_{min}, the rise in the remaining amplitudes results in the differential cross section turnover. Since we consider only pion exchange, we have no WSNZ dips in the range $|t_{min}| < |t| < 1.0\ (\mathrm{GeV}/c)^2$. A similar effect can be seen in the two-body exclusive production of the f^o[32].

In Figs. 5.3 and 5.5 we have plotted the density matrix elements in the Gottfried-Jackson frame. In a Mueller-Regge model with Reggeized pion exchange[41] we would get the result $\rho_{00} = 1$ and $\rho_{11} = \mathrm{Re}\ \rho_{2-1} = 0$ for all t and all M^2/s. With the addition of absorption corrections ρ_{00} shows strong dependence on both t and M^2/s while ρ_{11} and $\mathrm{Re}\rho_{2-1}$ still remain close to their unabsorbed predictions. In particular, ρ_{00} varies between 1 and 0 as t varies between t_{min} and $t_{min} - 0.5\ (\mathrm{GeV}/c)^2$ for fixed M^2/s and between the same limits as M^2/s varies between the edge of phase space and 0.01 for fixed t. ρ_{00} is dominated by H^{00}_{abs} so that the position of the zeros in H^{00}_{abs} corresponds to the position of the zeros in ρ_{00} in the c.m. frame.

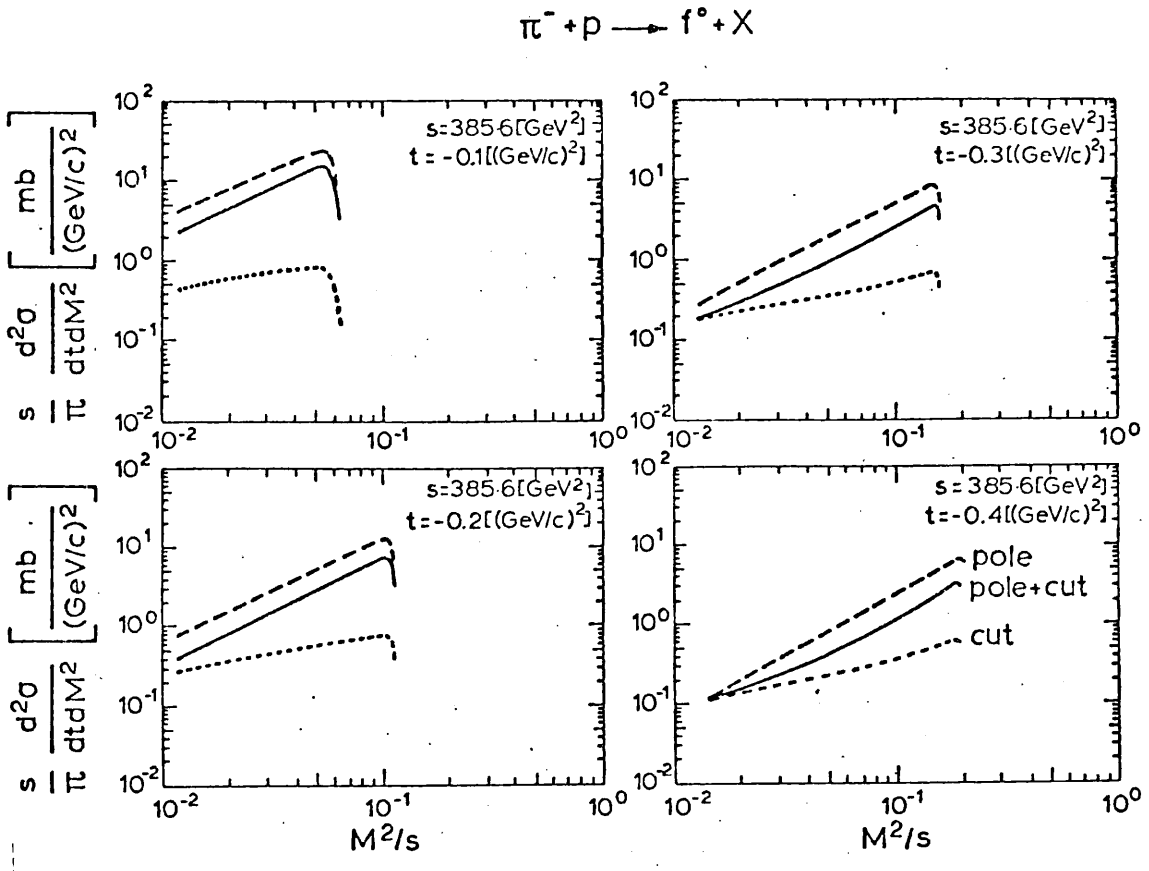

Fig. 5.4 The invariant differential cross sections for fixed t.

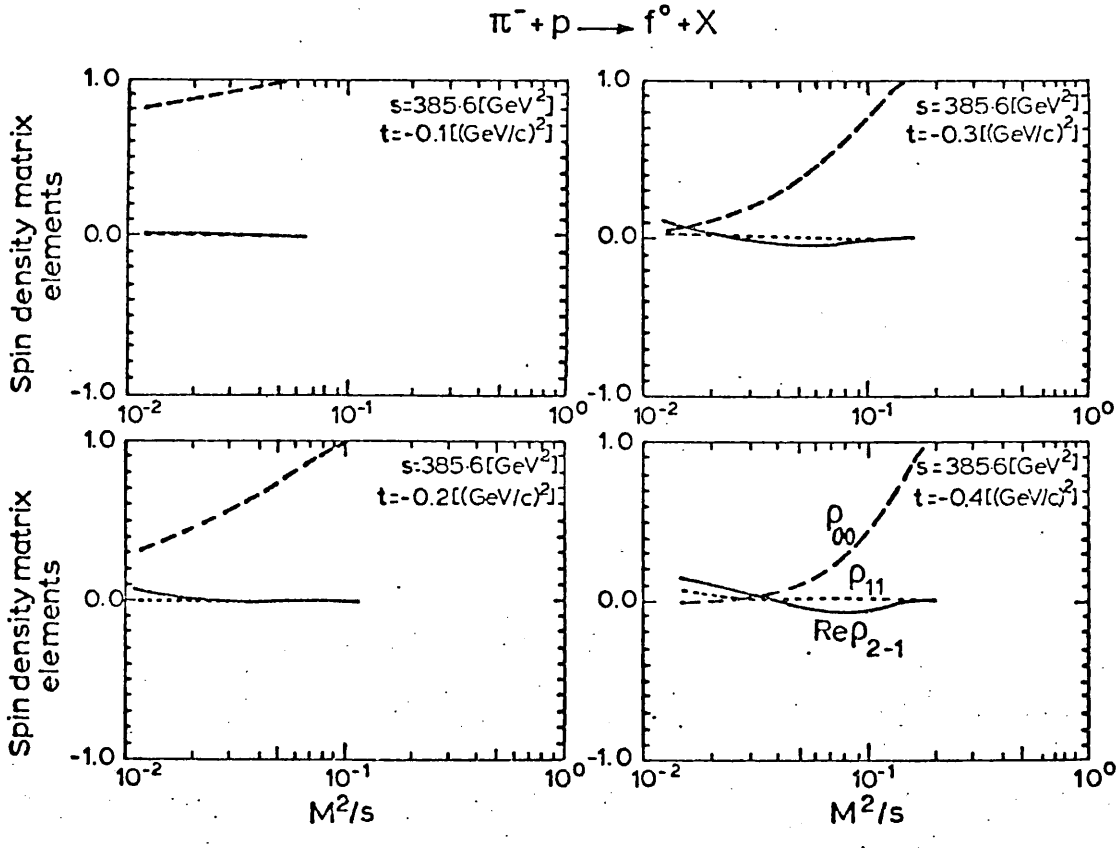

Fig. 5.5 The decay density matrix elements for fixed t.

In conclusion we state that our model for including absorption corrections in the Mueller-Regge formalism leads to the very definite prediction, which is independent of the overall normalization of our amplitudes, that ρ_{00} will be a strong function of both t and M^2/s. An experiment of not very high statistics, some of which are currently in progress, could verify this prediction. Moreover, for the differential cross section, our prediction after carrying out the integration over missing mass squared, is comparable to the experimental results at 16 GeV/c[71].

$$(p^2 - m^2)\,\Phi_{\mu_1 \cdots \mu_J}(\lambda,p) = 0\,, \quad g^{\mu_i\mu_k}\Phi_{\mu_1 \cdots \mu_i \cdots \mu_k \cdots \mu_J}(\lambda,p) = 0\,,$$

and

$$p^{\mu_i}\,\Phi_{\mu_1 \cdots \mu_i \cdots \mu_J}(\lambda,p) = 0\,, \quad (i,k = 1,2,\ldots,J)\,;$$

where, as before, λ represents the helicity states. The wave functions are normalized according to

$$\Phi^{*}_{\mu_1 \cdots \mu_J}(\lambda,p)\;\Phi^{\mu_1 \cdots \mu_J}(\lambda',p) = (-1)^J\,\delta_{\lambda\lambda'}.$$

Particle with Half-Integer Spin $J + \frac{1}{2}$:

The half-integer spin $J + \frac{1}{2}$ states are described by the direct product of the integer spin J tensor representation and the Dirac spinor representation $(\frac{1}{2},0) \oplus (0,\frac{1}{2})$. However, this spin addition results in spins $J + \frac{1}{2}$ and $J - \frac{1}{2}$, the latter spin state can be eliminated by the appropriate projection conditions. The wave functions must satisfy the equations of motion

$$(\not{p} - m)u_{\mu_1 \cdots \mu_J}(\lambda,p) = 0 \text{ and } \gamma^{\mu}\,u_{\mu\mu_2 \cdots \mu_J}(\lambda,p) = 0\,;$$

and the normalization

$$\bar{u}_{\mu_1 \cdots \mu_J}(\lambda,p)\;u^{\mu_1 \cdots \mu_J}(\lambda',p) = (-1)^{J-\frac{1}{2}}\,2m\,\delta_{\lambda\lambda'}\,;$$

with $\bar{u} = u^{\dagger}\gamma_o$. The projection operators $\Lambda(p)$ consist of the symmetrized products of those already found for spin 1 and spin $\frac{1}{2}$. As examples of the last two paragraphs we give:

Spin 3/2 Particle:

Equations of motion are

$$(\not{p} - m)^{\beta}_{\alpha}\,u_{\beta\mu}(\lambda,p) = 0 \text{ and } (\gamma^{\mu})^{\beta}_{\alpha}\,u_{\beta\mu}(\lambda,p) = 0$$

and the projection operator is

$$\Lambda_{\alpha\mu,\ \nu}^{\ \beta}(p) = \left(\frac{\not{p}+m}{2m}\right)_{\alpha}^{\beta}\left(-g_{\mu\nu} + \frac{1}{3}\gamma_\mu\gamma_\nu + \frac{2\,p_\mu p_\nu}{3m^2} - \frac{p_\mu\gamma_\nu - p_\nu\gamma_\mu}{3m}\right) .$$

Spin 2 Particles:

$$(p^2 - m^2)\,\Phi_{\mu\nu}(\lambda,p) = 0,\ \Phi_{\mu\mu}(\lambda,p) = 0 \text{ and } p^\mu\,\Phi_{\mu\nu}(\lambda,p) = 0$$

are the equations of motion and

$$\Lambda_{(\mu\nu),(\kappa\lambda)}(p) = \tfrac{1}{2}\left[\left(-g_{\mu\kappa} + \frac{p_\mu p_\kappa}{m^2}\right)\left(-g_{\nu\mu} + \frac{p_\nu p_\lambda}{m^2}\right)\right] + \left[\kappa \leftrightarrow \lambda\right] - \frac{2}{3}\left[\kappa \leftrightarrow \nu\right],$$

is the projection operator.

A.2. Some Useful Mathematical Formulae

Fourier-Bessel or Hankel transform[73]

The Fourier-Bessel transform is given by

$$F(b) = \int_0^\infty J_\nu(b\tau)\ Q(\tau)\ \tau\ d\tau,$$

with the inverse transform

$$Q(\tau) = \int_0^\infty J_\nu(b\tau)\ F(b)\ b\ db,$$

where J_ν is the Bessel function of the first kind and $\nu > -1$.

The orthogonality condition for Bessel functions of first kind reads

$$\int_0^\infty J_\nu(b\tau)\ J_\nu(b'\tau)\ \tau d\tau = \frac{1}{b}\,\delta(b' - b).$$

The following integrals[74] are useful for calculations in the last three chapters

$$\int_0^\infty b\ db\ J_\nu(b\tau)\ J_\nu(b\tau')\ \exp(-\lambda\ b^2)$$

$$= \frac{1}{2\lambda}\exp\left(-\frac{\tau^2+\tau'^2}{4\lambda}\right) I_\nu\left(\frac{\tau\tau'}{2\lambda}\right),$$

Spin 1

The polarization vector of a spin 1 particle at rest is given by

$$\varepsilon^{\mu}(\pm 1,0) = \frac{1}{\sqrt{2}}\begin{pmatrix} 0 \\ 1 \\ \pm i \\ 0 \end{pmatrix}, \quad \varepsilon^{\mu}(0,0) = \begin{pmatrix} 0 \\ 0 \\ 0 \\ 1 \end{pmatrix}.$$

The helicity polarization vectors of a spin 1 particle with momentum q, which makes an angle θ w.r.t.+z-axis, are obtained by a Lorentz transformation followed by a rotation and are given by

$$\varepsilon^{\mu}(\pm 1,q) = \frac{1}{\sqrt{2}}\begin{pmatrix} 0 \\ \cos\theta \\ \pm i \\ -\sin\theta \end{pmatrix}, \quad \varepsilon^{\mu}(0,q) = \frac{1}{m_V}\begin{pmatrix} q \\ E\sin\theta \\ 0 \\ E\cos\theta \end{pmatrix}$$

where the mass and energy of particle are denoted by m_V and E respectively.

Spin 2

The wave functions of a spin 2 particle with momentum q moving in the direction θ w.r.t.+z-axis are given by

$$\phi_{\mu\nu}(\pm 2,q) = \varepsilon_{\mu}(\pm 1,q)\,\varepsilon_{\nu}(\pm 1,q),$$

$$\phi_{\mu\nu}(\pm 1,q) = \frac{1}{\sqrt{2}}\left(\varepsilon_{\mu}(\pm 1,q)\varepsilon_{\nu}(0,q)+\varepsilon_{\mu}(0,q)\varepsilon_{\nu}(\pm 1,q)\right),$$

$$\phi_{\mu\nu}(0,q) = \frac{1}{\sqrt{6}}\left(2\,\varepsilon_{\mu}(0,q)\varepsilon_{\nu}(0,q)+\varepsilon_{\mu}(-1,q)\varepsilon_{\nu}(+1,q)+\varepsilon_{\mu}(+1,q)\varepsilon_{\nu}(-1,q)\right)$$

where the ε_{μ}'s are defined above in section on Spin 1.

Note that the spin 2 wave functions are expressed in terms of their constituent vector wave functions. This is only because the vector wave functions and their properties are more familiar, which will perhaps make the evaluation of the transition amplitudes easier.

B.3. Normalization

A high energy one-particle-inclusive reaction in which the collision between particles a and b produces particle c and any other thing is written as $a + b \to c + X$ or as (ab;c). The 4-momenta (energies) of a, b and c are denoted by $p_a(E_a)$, $p_b(E_b)$ and $p_c(E_c)$, respectively. In this section all spin indices are suppressed and it is assumed that the summation over final spin states and averaging over initial spin states has been carried out. The one-particle-inclusive cross section is

$$\langle n \rangle \sigma_{ab}^{c} = \frac{1}{2s} \int \frac{d^3p_c}{(2\pi)^3 2E_c} \frac{d^3p_X}{(2\pi)^3 2E_X} (2\pi)^2 \delta^4(p_a+p_b-p_c-p_X) \cdot$$

$$\cdot \left| \langle c,X \mid A(s,p_c,p_X,t) \mid a,b \rangle \right|^2 ,$$

where $\langle n \rangle$ is the multiplicity of c and X refers to anything. We know that the total cross section σ_{TOT} and d^3p_c/E_c are Lorentz invariants. Therefore it is possible to define a Lorentz invariant momentum distribution of the form

$$\frac{E_c \, d\sigma_{ab}^{c}}{d^3p_c} .$$

In the kinematical region $s >> M^2 >> m^2$, or the fragmentation region, one has the kinematical relation

$$E_c \frac{d\sigma_{ab}^{c}}{d^3p_c} = \frac{s}{\pi} \frac{d^2\sigma}{dt dM^2} ,$$

where s and t are the usual Mandelstam variables and M is the missing mass. Moreover, from energy-momentum conservation in this region, we know that there can be at most one particle, so that $\langle n \rangle = 1$[27,40]. Hence the invariant differential cross section is defined by

$$\frac{s}{\pi}\frac{d^2\sigma}{dtdM^2} = \frac{1}{16\pi^2 s}\int d^4p_X\,\delta^4(p_a+p_b-p_c-p_X)\,\delta(p_X^2-M^2)$$

$$\cdot\,\theta(E_a+E_b-E_c)\,|\,<c,X\,|\,A(s,p_X,t)|a,b>\,|^2$$

$$= \frac{1}{16\pi^2 s}\,\delta\,((p_a+p_b-p_c)^2 - M^2)\;\theta\;(E_a+E_b-E_c)$$

$$\cdot\,|<c,\,X\,|\,A(s,t,M^2)\,|\,a,b>|^2\,,$$

with

$$\theta(x) = 1\,; \qquad x \geq 0\,,$$

$$= 0\,; \qquad x < 0.$$

A P P E N D I X C

STRUCTURE FUNCTIONS

Considering the nucleon-vector meson interaction, the most general symmetric tensor we can form from the available four-vectors is, after summing out the nucleon spin,

$$M^{\nu\nu'} = V_1 g^{\nu\nu'} + V_2 p^{\nu} p^{\nu'} + V_3 q^{\nu} q^{\nu'} + V_4 (p^{\nu} q^{\nu'} + q^{\nu} p^{\nu'})$$

where p and q are the nucleon and the vector meson four-momenta shown in Fig. C.1. For any vector meson this will be contracted with

$$\varepsilon_{\nu}^{\lambda *}(q) = \varepsilon_{\nu}^{*}(\lambda,q) \quad \text{and} \quad \varepsilon_{\nu'}^{\lambda}(q) = \varepsilon_{\nu'}(\lambda,q),$$

where the $\varepsilon(\lambda,q)$'s are defined in Appendix B, so that V_3 and V_4 are redundant. (Our choice of gauge invariant currents at the three-particle vertex ensures the validity of this arguement for our purposes.) The standard optical theorem gives us

$$\text{Flux.}\ \sigma_{TOT}(VN) = \text{Disc}_{s'\,|\,t'=0} \{\Sigma_{\lambda}\, \varepsilon_{\nu}^{\lambda *}(q) M^{\nu\nu'} \varepsilon_{\nu'}^{\lambda}(q)\}$$

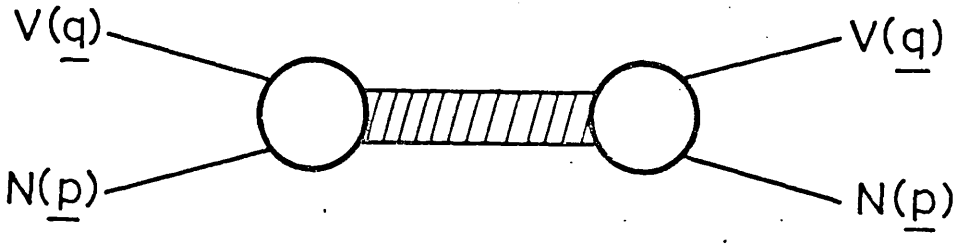

Fig. C.1. Nucleon-vector meson forward scattering

Using the vector meson wave functions

$$\varepsilon_{\nu}^{o}(q) = \frac{1}{m_V}(q,\ E \sin\theta, 0,\ E \cos\theta),$$

* Strictly speaking the factor $\sigma_{TOT}(VN) \equiv \frac{1}{3}(\sigma_{TOT}^{(0)}(VN) + 2\sigma_{TOT}^{(1)}(VN))$ should be replaced by $\sigma_{TOT}^{(0)}(VN) - \sigma_{TOT}^{(1)}(VN)$. For lack of experimental information on the total cross sections for the individual helicities $\lambda = 0$, $\lambda = 1$, we take the former expression as giving the correct order of magnitude.

$$\varepsilon_\nu^{\pm}(q) = (0; \mp \frac{1}{\sqrt{2}} (\cos\theta, \pm i, -\sin\theta))$$

$$= (0; \underline{U}^{\pm}(q)),$$

where $\underline{U}^{\pm}(q)$ are defined by this expression and satisfy $\underline{U}^{\pm}(q).\underset{\sim}{q}=0$, the normalization is

$$\sum_\lambda \varepsilon_\nu^{\lambda *}(q)\, g^{\nu\nu'}\, \varepsilon_{\nu'}^{\lambda}(q) = 3.$$

Then if we take

$$M^{\nu\nu'} = V_1\, g^{\nu\nu'} + V_2\, p^\nu p^{\nu'},$$

we have

$$2\,\Delta(s',m_V^2,m_N^2)\,\sigma_{TOT}(V\,N)$$

$$= \mathrm{Disc}_{s'}\big|_{t'=0} V_2(s',t') \left(\frac{\Delta(s',m_V^2,m_N^2)}{2m_V}\right)^2 + 3\,\mathrm{Disc}_{s'}\big|_{t'=0} V_1(s',t'),$$

or

$$\mathrm{Disc}_{s'} V_2 + \frac{12\,m_V^2}{\Delta^2(s',m_V^2,m_N^2)}\,\mathrm{Disc}_{s'} V_1 = \frac{8\,m_V^2}{\Delta(s',m_V^2,m_N^2)}\,\sigma_{TOT}(V\,N).$$

We note that the term involving V_2 (and hence $p_1^\nu p_1^{\nu'}$ in terms of our inclusive matrix element squared) will be multiplied by a factor of s^2 (via the $(p.p_1)^2$ term), and while $\mathrm{Disc}_{s'} V_1$ is allowed to be a factor of $(s')^2$ (where s' is identified with M^2) greater than $\mathrm{Disc}_{s'} V_2$, in the triple-Regge region this becomes a factor of $(M^2/s)^2$ which will be small.

Thus we will neglect V_1 and take *

$$\mathrm{Disc}_{s'} V_2 = \frac{8\,m_V^2}{\Delta(s',m_V^2,m_N^2)}\,\sigma_{TOT}(V\,N).$$

$$\phi_{++}^{\pi abs}(s,\tau,M^2) = \phi_{++}^{\pi}(s,\tau,M^2) - C\exp\left[-\frac{\tau^2}{4\lambda}\right]$$

$$\cdot\left(\sum_{i=1}^{4} p_{++}^{i}\left\{\left(\frac{\exp\left[\tau^2/4\lambda(4\lambda b_{1i}+1)\right]}{(4\lambda b_{1i}+1)}\left[1-\frac{4\lambda(4\lambda b_{1i}+1)+\tau^2}{8k^2(4\lambda b_{1i}+1)^2}\right]\right)+\eta_{\pi}(b_{1i}\rightarrow b_{2}i)\right\}\right),$$

$$\phi_{+-}^{\pi abs}(s,\tau,M^2) = \phi_{+-}^{\pi}(s,\tau,M^2) - C(\tfrac{\tau}{k})\exp\left[-\frac{\tau^2}{2k}\right]$$

$$\cdot\left(\sum_{i=1}^{4} p_{+-}^{i}\left\{\left[\frac{\exp\left[\tau^2/4\lambda(4\lambda b_{1i}+1)\right]}{(4\lambda b_{1i}+1)^2}\right]+\eta_{\pi}(b_{1i}\rightarrow b_{2i})\right\}\right),$$

$$\phi_{++}^{\rho abs}(s,\tau,M^2) = \phi_{++}^{\rho}(s,\tau,M^2) - C\exp\left[-\frac{\tau^2}{4\lambda}\right]$$

$$\cdot\left(\left\{\frac{\exp\left[\tau^2/4\lambda(4\lambda d_1+1)\right]}{(4\lambda d_1+1)}\left[R_{++}^{1}-\frac{(R_{++}^{1}+4R_{++}^{2})}{8k^2(4\lambda d_1+1)^2}(4\lambda\left[4\lambda d_1+1\right]+\tau^2)\right.\right.\right.$$

$$\left.\left.\left.+\frac{R_{++}^{2}}{16k^2(4\lambda d_1+1)^4}(\tau^4+16\tau^2\lambda\left[4\lambda d_1+1\right]+32\lambda^2\left[4\lambda d_1+1\right]^2)\right]\right\}+\eta_{\rho}\{d_1\rightarrow d_2\}\right),$$

and

$$\phi_{+-}^{\rho abs}(s,\tau,M^2) = \phi_{+-}^{\rho}(s,\tau,M^2) - C(\tfrac{\tau}{2k})\exp\left[-\frac{\tau^2}{4\lambda}\right]$$

$$\cdot\left[\left\{\frac{\exp\left[\tau^2/4\lambda(4\lambda d_1+1)\right]}{(4\lambda d_1+1)^2}\left[R_{+-}^{1}-\frac{R_{+-}^{2}}{2k^2}\frac{(\tau^2+8\lambda\left[4\lambda d_1+1\right])}{(4\lambda d_1+1)^2}\right]\right\}+\eta_{\rho}\{d_1\rightarrow d_2\}\right].$$

D.3. Absorbed Helicity Amplitudes for f^{o} Production

In order to give the final form of $A_{abs}^{\lambda c}$ and $A_{abs}^{\lambda' c}$ (see Chapter 5). Let us use the results of that chapter and define

$$f_i = \tfrac{1}{2}\left[a_i\alpha_{\pi}'\left(\frac{s}{M^2}\right)^{(\alpha_{o\pi}+\alpha' t_{min})}\right]\exp\left[b_i\, t_{min}\right],$$

$$b_{1i} = \frac{q}{k}\left[b_i + \alpha_{\pi}'\ln\left(\frac{s}{M^2}\right)\right],\quad b_{2i} = \frac{q}{k}\left[b_i + \alpha_{\pi}'\ln\left(\frac{s}{M^2}\right) - i\pi\alpha_{\pi}'\right],$$

$$\eta_\pi = \exp\left[- i\pi\,(\alpha_{o\pi}+\alpha'_\pi\, t_{min})\right],\quad C_1 = \frac{C}{2\lambda}\ \exp\left[-\frac{\tau^2}{4\lambda}\right],$$

$$d_{1i} = \frac{\tau^2}{16\lambda^2(\frac{1}{4\lambda}+b_{1i})},\quad d_{2i} = \frac{\tau^2}{16\lambda^2(\frac{1}{4\lambda}+b_{2i})},$$

$$e_{1i} = (\frac{1}{4\lambda}+b_{1i})^{-1},\quad e_{2i} = (\frac{1}{4\lambda}+b_{2i})^{-1},$$

with $t_{min} = m_a^2 + m_c^2 - 2E_a E_c + 2qk$. Then we have

$$A_{abs}^{\lambda_c=2} = A_{abs}^{\lambda'=2} = A^2 - C_1 \sum_{i=1}^{4} f_i \left[(\frac{\tau^2 e_{1i}^3}{64\lambda^2}\exp\left[d_{1i}\right]\{1 - \frac{e_{1i}}{4k^2}\left[3 + d_{1i}\right] + \frac{e_{1i}^2}{64k^2}\left[d_{1i}^2 + 8d_{1i} + 12\right]\}) + \eta_\pi\,(d_{1i}\to d_{2i},\ e_{1i}\to e_{2i})\right],$$

$$A_{abs}^{\lambda_c=1} = -A_{abs}^{\lambda'=-1} = A^1 - C_1\frac{\tau}{8\lambda m_c}\sum_{i=1}^{4} f_i\Big[(e_{1i}^2\exp\left[d_{1i}\right]\{qE_a - kE_c - \frac{(qE_a-5kE_c)}{8k^2}\cdot e_{1i}\left[d_{1i}+2\right] - \frac{(qE_a+7kE_c)}{128k^4}\,e_{1i}^2\left[d_{1i}^2 + 6d_{1i} + 6\right]\}) + \eta_\pi(d_{1i}\to d_{2i},\ e_{1i}\to e_{2i})\Big],$$

$$A_{abs}^{\lambda_c=0} = A_{abs}^{\lambda'=0} = A^o - C_1\,(-\frac{1}{\sqrt{6}m_c^2})\sum_{i=1}^{4} f_i\Big[(\frac{1}{2}e_{1i}\exp\left[d_{1i}\right]\{2\left[qE_a - kE_c\right]^2 + \left[2E_aE_c\frac{q}{k} - 2E_c^2 - m_c^2\right]e_{1i}\left[1+d_{1i}\right] + \frac{(2E_c^2+m_c^2)}{4k^2}\,e_{1i}^2\left[d_{1i}^2 + 4d_{1i} + 2\right] - \frac{m_c^2}{64k^4}\,e_{1i}^3\left[d_{1i}^3 + 9d_{1i}^2 + 18d_{1i} + 16\right]\}) + \eta_\pi(d_{1i}\to d_{2i},\ e_{1i}\to e_2 i)\Big].$$

REFERENCES

1. For a review of multiparticle production see, e.g.,
   L. Van Hove, Phys. Reports 1C, 347 (1971);
   D. Horn, Phys. Reports 4C, 1 (1972).
2. W.R. Fraser, L. Ingber, C.H. Mehta, C.H. Poon, D. Silverman,
   K. Stowe, P.D. Ting and H.J. Yesian, Rev. Mod. Phys. 44, 284 (1972).
3. G. Giacomelli, Phys. Reports 23C, 123 (1976).
4. A.R. White, Proc. of Les Houches June Institute 1975, North-
   Holland, Amsterdam (1976).
5. For a review of inclusive approach see, e.g.,
   S. Humble, Introduction to Particle Production in Hadron Physics,
   Academic Press, New York (1974).
6. For a review of inclusive data see, e.g.,
   K. Zalewski, I-93, Proc. XVIIth Int. Conf. on High Energy Physics,
   London (1974), Ed. J.R. Smith;
   J. Whitmore, Phys. Reports 10C, 273 (1974);
   G. Giacomelli, A.F. Greene and J.R. Sandford, Phys. Reports
   19C, 169 (1975).
7. R.P. Feynman, Phys. Rev. Letters 23, 1415 (1969).
8. L. Bertocchi, S. Fubini and M. Tonin, Nuovo Cim. 25, 626 (1962);
   D. Amati, S. Fubini and A. Stanghellini, Nuovo Cim. 26, 896 (1962).
9. L.G. Ratner, R.J. Ellis, G. Vannini, B.A. Babcock, A.D. Krisch
   and J.B. Roberts, Phys. Rev. Letters 27, 68 (1971).
10. J. Benecke, T.T. Chou, C.N. Yang and E. Yen, Phys. Rev. 188, 2159 (1969).
11. A.H. Mueller, Phys. Rev. D2, 2963 (1970).
12. R.G. Roberts, XIVth Scottish Universities Summer School, Aug. 1973,
    Eds. R.L. Crawford and R. Jennings, Academic Press, London (1974).
13. R. Slansky, Phys. Reports 11C, 99 (1974).

14. C.-I. Tan, Phys. Rev. D4, 2412 (1972);
K.E. Cahill and H.P. Stapp, Phys. Rev. D6, 1007 (1972);
H.P. Stapp, Proc. of Les Houches June Institute 1975,
North-Holland, Amsterdam (1976).

15. E. Byckling and K. Kajantie, Particle Kinematics, John Wiley,
London (1973).

16. R.J. Eden, P.V. Landshoff, D.I. Olive and J.C. Polkinghorne,
The Analytic S-Matrix, Cambridge University Press (1966).

17. H.D.I. Abarbanel and D.J. Gross, Phys. Rev. Letters 26, 732 (1971);
G.A. Ringland, R.J.N. Phillips and R. Warden, Phys. Letters
40B, 239 (1972).

18. J. Randa and Donnachie, Nucl. Phys. B109, 495 (1976).

19. J.P. Ader, C. Meyers and Ph. Salin, Nucl. Phys. B47, 397 (1972);
Nucl. Phys. B82, 237 (1974).

20. J.F. Owens, Phys. Letters, 63B, 341 (1976).

21. For a review see,e.g.,
J.E. Young, Revista del Nuovo Cim. 2, 88 (1972);
R.C. Brower, C.E. De Tar and J.H. Weis, Phys. Reports 14C,
257 (1974).

22. C.E. DeTar and J.H. Weis, Phys. Rev. D4, 3141 (1971);
C.E. Jones, F.E. Low and J.E. Young, Phys. Rev. D4, 2358 (1971);
P. Goddard and A.R. White, Nuovo Cim. 1A, 645 (1971);
H.D.I. Abarbanel and A. Schwimmer, Phys. Rev. D6, 3018 (1972);
N.S. Craigie and G. Kramer, Nucl. Phys. B82, 69 (1974).

23. C.E. De Tar, C.E. Jones, F.E. Low, C.-I. Tan, J.H. Weis and
J.E. Young, Phys. Rev. Letters 26, 675 (1971).

24. H.M. Chan, H.I. Miettinen, D.P. Roy, and P. Hayer, Phys. Letters
40B, 406 (1972).

25. H.M. Chan and P. Hoyer, Phys. Letters 36B, 79 (1971);
P.G.O. Freund, Phys. Rev. Letters 20, 235 (1968);
H. Harari, Phys. Rev. Letters 20, 1395 (1968).

26. H.M. Chan, C.S. Hsue, C. Quigg and J.M. Wang, Phys. Rev. Letters 26, 672 (1971).

27. D. Horn and F. Zachariasen, Hadron Physics at Very High Energies, Benjamin, New York (1973).

28. R. Delbourgo, Elementary Particle Symmetries, D.I.C. Lecture Notes, Imperial College, London (1972-1973).

29. A. Salam, R. Delbourgo and J. Strathdee, Proc. Roy. Soc. A, 284, 146-158 (1965);
R. Delbourgo and A. Salam, Phys. Rev. 186, 1516 (1969).

30. J.D. Jackson, Duality and Exchange Degeneracy in High-Energy Phenomenology, Invited Paper presented at the Int. Conf. on Duality and Symmetry in Hadron Physics, Tel-Aviv (1971).

31. S.A. Adjei, P.A. Collins, B.J. Hartley, K.J.M. Moriarty and R.W. Moore, Ann. of Phys. (N.Y.) 75, 405 (1973).

32. P.A. Collins, B.J. Hartley, R.W. Moore and K.J.M. Moriarty, J. Phys. A6, 506 (1973).

33. R.G. Sachs, Phys. Rev. 126, 2256 (1962).

34. G. Ebel, H. Pilkuhn and F. Steiner, Proc. of the Int. Conf. on Elementary Particles, Lund (1969).

35. V.S. Barashenkov, Interaction Cross sections of Elementary Particles, Israel Program for Scientific Translation, Jerusalem (1968).

36. N.S. Craigie, G. Kramer and J. Körner, Nucl. Phys. B68, 509 (1974).

37. J.J. Sakurai and D. Schildknecht, Phys. Letters 40B, 121 (1972).

38. A. Dar, K.J.M. Moriarty and J. Tran Thanh Van, Acta. Phys. Austr. 43, 99 (1975).

39. H.J. Lipkin and F. Scheck, Phys. Rev. Letters 16, 71 (1966).

40. R.N. Cahn, Phenomenology of Inclusive Reactions, (1972 Ph.D. Thesis), LBL-1007.

41. P. Choudhury, K.J.M. Moriarty, J.H. Tabor and Ungkitchanukit, A Study of Inclusive Δ-Production, Acta. Phys. Austr. 47, (1977); A Study of Inclusive Vector and Tensor Meson Production in the Triple-Regge Region, Acta. Phys. Austr. 46,(1977).

42. B. Robinson, K. Abe, J. Carr, J. Keyne, A. Pagnamenta, F. Sannes, I. Siotis and R. Stanek, Phys. Rev. Letters 34, 1475 (1975).

43. J. Engler, B. Gibbard, W. Isenbeck, F. Mönnig, J. Mortiz, K. Pack, K.H. Schmidt, D. Wegener, W. Bartel, W. Flauger and H. Schopper, Nucl. Phys. B84, 70 (1975).

44. K.J.M. Moriarty, J.H. Tabor and A. Ungkitchanukit, Acta. Phys. Austr. 45, 325 (1976);
A. Ungkitchanukit, Particle Production at High Energies, Ph.D. Thesis, Royal Holloway College, University of London (1976).

45. P.D.B. Collins and E.J. Squires, Regge Poles in Particle Physics, Springe, Berlin (1968);
P.D.B. Collins, Phys. Reports 1C, 103 (1971).

46. R.W.B. Ardill, P. Choudhury, K.J.M. Moriarty and A. Ungkitchanukit, Acta. Phys. Austr. 46, 27 (1976).

47. K.J.M. Moriarty, J.P. Rad, J.H. Tabor and A. Ungkitchanukit, Acta. Phys. Austr. 46, 105 (1977).

48. J. Pumplin, Phys. Rev. D13, 1249 (1976).

49. J. Pumplin, Phys. Rev. D13, 1262 (1976);
F.E. Paige and D.P. Sidhu, Phys. Rev. D13, 3015 (1976).

50. N.S. Craigie and G. Kramer, Nucl. Phys. B75, 509 (1974).

51. K. Ahmed, N.S. Craigie, J. Körner and G. Kramer, Nucl. Phys. B106, 275 (1976).

52. F.E. Paige and D.P. Sidhu, Phys. Rev. D14, 2307 (1976).